AD-A141 016 COMPUTER-AIDED DESIGN OF MILLIMETER WAVE E-PLANE FILTERS(U) TEXAS UNIV AT AUSTIN MICROWAVE LAB Y C SHIH ET AL. 01 MAR 84 MW-84-1 ARO-17735.33-EL 1/1

UNCLASSIFIED DAAG29-81-K-0053 F/G 9/5 NL

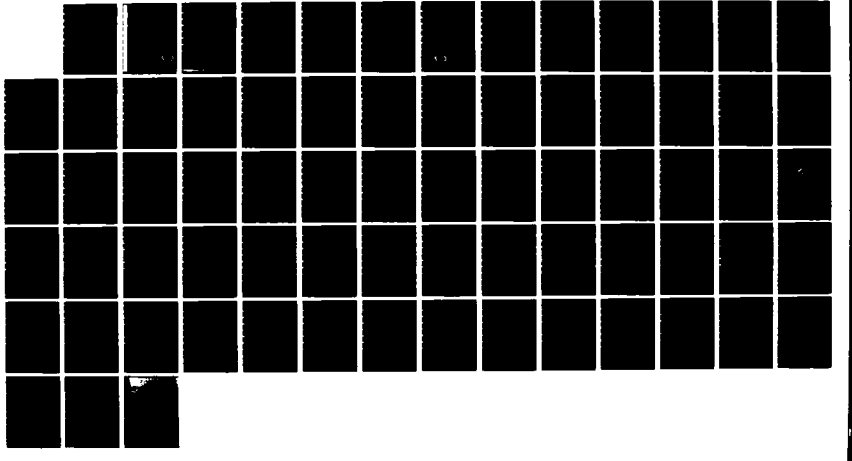

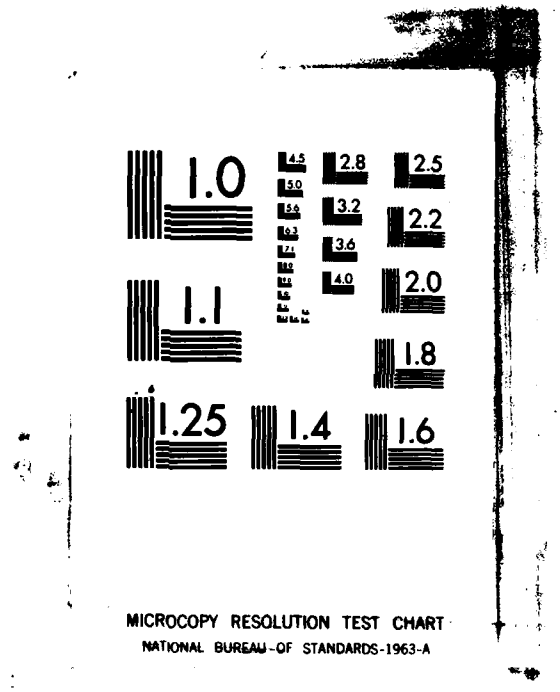

MICROWAVE LABORATORY REPORT No. 84-1

COMPUTER-AIDED DESIGN OF MILLIMETER WAVE E-PLANE FILTERS

TECHNICAL REPORT

YI-CHI SHIH AND TATSUO ITOH

MARCH 1, 1984

U.S. ARMY RESEARCH OFFICE

CONTRACT NO. DAAG29-81-K-0053

UNIVERSITY OF TEXAS

DEPARTMENT OF ELECTRICAL ENGINEERING

AUSTIN, TX 78712

APPROVED FOR PUBLIC RELEASE;

DISTRIBUTION UNLIMITED

THE FINDINGS IN THIS REPORT ARE NOT TO BE CONSTRUED AS AN OFFICIAL DEPARTMENT OF THE ARMY POSITION, UNLESS SO DESIGNATED BY OTHER AUTHORIZED DOCUMENTS.

Unclassified

SECURITY CLASSIFICATION OF THIS PAGE (When Data Entered)

REPORT DOCUMENTATION PAGE		READ INSTRUCTIONS BEFORE COMPLETING FORM
1. REPORT NUMBER MW No. 84-1	2. GOVT ACCESSION NO. AD-A141016	3. RECIPIENT'S CATALOG NUMBER
4. TITLE (and Subtitle) COMPUTER-AIDED DESIGN OF MILLIMETER WAVE E-PLANE FILTERS		5. TYPE OF REPORT & PERIOD COVERED Technical Report 6. PERFORMING ORG. REPORT NUMBER
7. AUTHOR(s) Yi-Chi Shih and Tatsuo Itoh		8. CONTRACT OR GRANT NUMBER(s) DAAG 29-81-K-0053
9. PERFORMING ORGANIZATION NAME AND ADDRESS University of Texas at Austin Department of Electrical Engineering Austin, Texas 78712		10. PROGRAM ELEMENT, PROJECT, TASK AREA & WORK UNIT NUMBERS
11. CONTROLLING OFFICE NAME AND ADDRESS U. S. Army Research Office Post Office Box 12211 Research Triangle Park, NC 27709		12. REPORT DATE March 1, 1984 13. NUMBER OF PAGES
14. MONITORING AGENCY NAME & ADDRESS(if different from Controlling Office)		15. SECURITY CLASS. (of this report) Unclassified 15a. DECLASSIFICATION/DOWNGRADING SCHEDULE

16. DISTRIBUTION STATEMENT (of this Report)

Approved for public release: distribution unlimited.

17. DISTRIBUTION STATEMENT (of the abstract entered in Block 20, if different from Report)

N/A

18. SUPPLEMENTARY NOTES

THE VIEW, OPIN[illegible] IN THIS REPORT ARE THOSE OF [illegible] AND SHOULD NOT BE CONSTRUED AS AN OFFICIAL DEPARTMENT OF THE [illegible] POSITION, POLICY, OR DECISION, UNLESS SO DESIGNATED BY OTHER DOCUMENTATION.

19. KEY WORDS (Continue on reverse side if necessary and identify by block number)

E-plane filters, finline, waveguide, residue-calculus, generalized scattering matrix, optimization.

20. ABSTRACT (Continue on reverse side if necessary and identify by block number)

This study presents a computer-aided design algorithm developed for a class of E-plane waveguide filters. The filter structure is composed of an integrated finline circuit in a waveguide. The circuit consists of several resonators seperated by inductive strips. The analysis portion of the algorithm is based on the residue-calculus technique and a generalized scattering parameter method. It is mathematically exact and numerically very efficient because the convergence is guaranteed. Filters designed

DD FORM 1 JAN 73 1473 EDITION OF 1 NOV 65 IS OBSOLETE

Unclassified

SECURITY CLASSIFICATION OF THIS PAGE (When Data Entered)

with this method are fabricated and tested at Ka-band. Good agreement with design is obtained.

MICROWAVE LABORATORY REPORT No. 84-1

COMPUTER-AIDED DESIGN OF MILLIMETER WAVE E-PLANE FILTERS

TECHNICAL REPORT

YI-CHI SHIH AND TATSUO ITOH

MARCH 1, 1984

U.S. ARMY RESEARCH OFFICE

CONTRACT NO. DAAG29-81-K-0053

UNIVERSITY OF TEXAS

DEPARTMENT OF ELECTRICAL ENGINEERING

AUSTIN, TX 78712

COMPUTER-AIDED DESIGN OF MILLIMETER WAVE

E-PLANE FILTERS

ABSTRACT

This study presents a computer-aided design algorithm developed for a class of E-plane waveguide filters. The filter structure is composed of an integrated finline circuit in a waveguide. The circuit consists of several resonators seperated by inductive strips. The analysis portion of the algorithm is based on the residue-calculus technique and a generalized scattering parameter method. It is mathematically exact and numerically very efficient because the convergence is guaranteed. Filters designed with this method are fabricated and tested at Ka-band. Good agreement with design is obtained.

TABLE OF CONTENTS

LIST OF TABLES

LIST OF FIGURES

Figure

I. INTRODUCTION

Waveguide filters using conventional inductive elements such as rods, transverse strips, and transverse diaphrams are difficult to produce at low cost and large quantities because of their complicated structures. Microstrip circuits have been used to solve this problem. However, these circuits are typically lossy, especially at millimeter-wave frequencies. A number of low-loss waveguide filters have been proposed recently [1,2,3,4,5] that are composed of printed circuits inserted in the waveguide parallel to the E-plane as shown in Fig. 1. The circuits are designed either on a metal sheet [1,2] or on a bilateral finline [3,4,5]. In these structures, the slot widths are equal to the waveguide height; in effect, the circuits consist of several resonators separated by printed inductive strips. Since the structures involve only straight line shapes and are amenable to photolithographic techniques, they are highly suitable for mass production.

In the previous works, most of the design procedures are based on various network-synthesis techniques where the inductive strips are represented by equivalent T-networks. The equivalent circuit parameters were obtained either by measurements [3] or by analytical methods such as mode matching techniques [2,4] and variational methods [1]. Although these procedures are accurate enough for some designs, the equivalent circuit approach neglects the effect of higher-order mode couplings between the strips. The

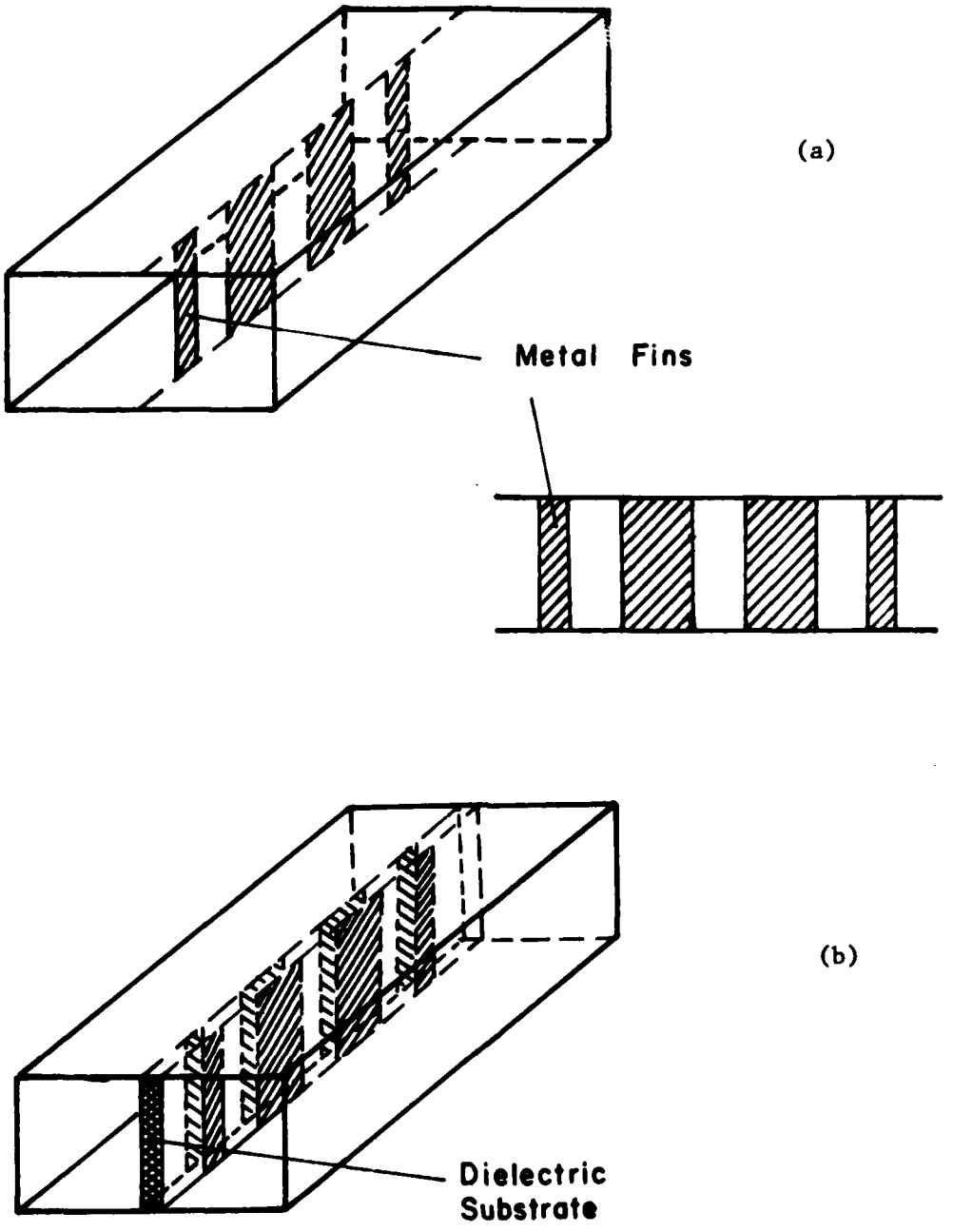

Fig. 1. E-plane waveguide filters. (a) Metal sheet, (b) Bilateral fineline.

neglect of this effect causes a bandwidth shrinkage and higher passband ripples in the filter response. To alleviate this problem, Arndt, et al. [5] have proposed a computer-aided design (CAD) procedure that takes into account the higher-order mode propagation for design of the bilateral filters. Their analysis is based on a mode matching technique that involves a number of matrix inversions. The matrix size must be made large to obtain accurate results, and as a result, the analysis becomes inefficient and may suffer the problem of relative convergence [6].

In this study, a new efficient CAD algorithm is developed for a class of E-plane bandpass filters [7]. A unified treatment is introduced that applies not only to purely metallic E-plane circuits and bilateral finline circuits but also to unilateral and insulated finline circuits (Fig. 2). Since the analysis portion of this algorithm is based on the residue-calculus technique [8] and a generalized scattering parameter method [9,10], it is mathematically exact and numerically very efficient because the convergence is guaranteed.

In the next chapter, the analysis is performed on a lossless structure with infinitesimally thin conductive sheets. The residue-calculus technique is first applied to obtain closed-form expressions for the scattering parameters of a single junction created by a semi-infinite septum in the waveguide. Then the composite scattering parameters of the filter structure are obtained using

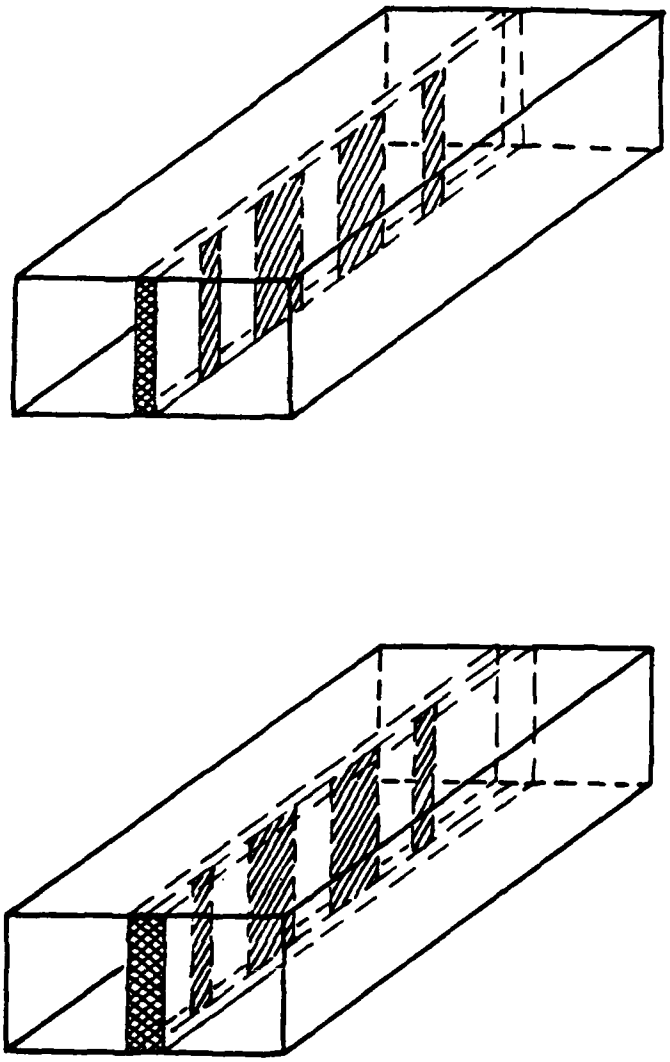

Fig. 2. E-plane waveguide filters. (a) Unilateral finline, (b) Insulated finline.

the generalized scattering matrix method that takes into account the interaction between junctions by the fundamental mode and all the higher-order evanescent modes. Finally, based on this analysis procedure, an optimization computer program is used to design filters for a given performance parameters. Filters designed with this method are fabricated and tested in Ka band [7]. Good agreement with design is obtained.

In the subsequent chapter, the effect due to the thickness of the strips is discussed. Based on the results in the previous analysis, the generalized scattering matrix method is applied again to obtain the scattering parameters for junctions created by septa of finite thickness. By taking into account the metal thickness, this analysis yields results in good agreement with experiments.

II. COMPUTER-AIDED DESIGN PROCEDURE

The CAD program consists of an analysis routine and an optimization routine. The analysis is carried out in three steps. First, a limiting case of a single junction created by a semi-infinite septum in a waveguide is analyzed. This structure may be analyzed exactly using the residue-calculus technique to obtain a closed-form expression for the scattering matrix. The second step is to calculate the scattering parameters for a finite-length septum. This is done by placing two junctions back-to-back and utilizing the concept of the generalized scattering matrix that

takes into account the interaction between junctions by the propagating modes and all the evanescent modes. Finally, several septa are combined to form a filter circuit. The total scattering parameters of the composite structure are obtained by repeating the procedure in the last step.

Based on the analysis, an objective function is defined and used in an optimization routine. The optimization routine varies the input parameters until the objective, i.e., the desired value of the insertion loss for a given bandwidth, is achieved. Since the coupling effects and frequency-dependent properties of the dominant mode, as well as higher-order modes, are considered in the analysis, the design procedure yields accurate results. In addition, a wider range of filter performance may be obtained through the optimization procedure.

A. Step 1 -- Semi-Infinite Septum

Let us consider an infinitesimally thin semi-infinite septum in a waveguide inhomogeneously filled with four dielectric slabs as shown in Fig. 3. This is a generalized structure for which values of the thickness and dielectric constant of each layer can be chosen to represent the structures in Fig. 1 and 2. (Note that for the case of bilateral finlines, a magnetic wall is introduced at the center of the waveguide and only the region above the magnetic wall is considered. Such a region represents the upper half of the bilateral finline due to the symmetry of the structure.) It is then

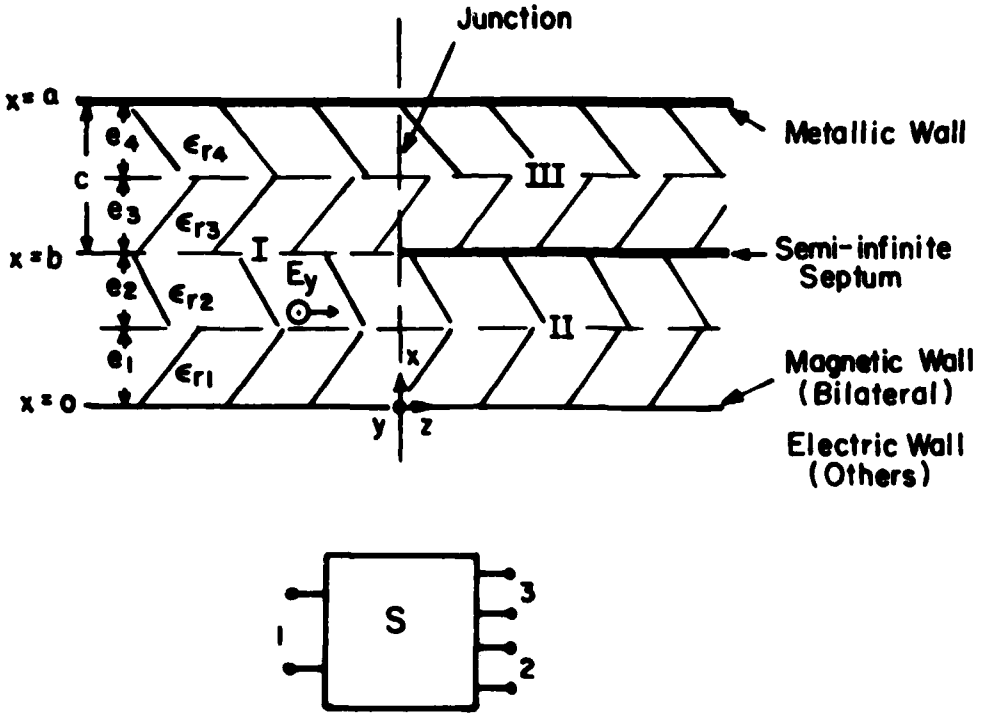

$$[S] = \begin{bmatrix} [S_{11}] & [S_{12}] & [S_{13}] \\ [S_{21}] & [S_{22}] & [S_{23}] \\ [S_{31}] & [S_{32}] & [S_{33}] \end{bmatrix}$$

Fig. 3. Characterization of semi-infinite septum.

subdivided into three regions at the junction z = 0, with each region consisting of a uniform waveguide which possesses known eigenmodes and corresponding propagation constants.

When a TE_{po}-type wave strikes on the junction, the excited fields are composed of the TE_{no}-type waves since there are no structural variations in the y-direction. Therefore, the existing modal fields consist of only E_y, H_x and H_z components. The total fields in each region are then expanded in terms of the orthonormal eigenmodes as

$$E_{iy} = A'_{ip}\phi_{ip}(x)\, e^{-\gamma_{ip}z} + \sum_{n=1}^{\infty} A_{in}\phi_{in}(x)\, e^{+\gamma_{in}z} \quad , \; i = 1,2,3 \qquad (1)$$

where $\{A_{in}\}$ are unknown coefficients and A'_{ip} is the amplitude of the incident wave from the i-th region; the expressions for the mode function $\phi_{in}(x)$ and the propagation constant γ_{in} are given in Appendix A for different structures. The continuity condition at z = 0 requires that the tangential electric field (E_y) and magnetic field ($H_x = \frac{1}{j\omega\mu_o}\frac{\partial E_y}{\partial z}$) be continuous. This leads to the following relations:

$$A'_{1p}\phi_{1p}(x) + \sum_{n=1}^{\infty} A_{1n}\phi_{1n}(x) = \begin{cases} A'_{2p}\phi_{2p}(x) + \sum_{n=1}^{\infty} A_{2n}\phi_{2n}(x) & , \; 0 < x < b \\ A'_{3p}\phi_{3p}(x) + \sum_{n=1}^{\infty} A_{3n}\phi_{3n}(x) & , \; b < x < a \end{cases} \qquad (2a)$$

$$-\gamma_{1p}A'_{1p}\phi_{1p}(x) + \sum_{n=1}^{\infty} \gamma_{1n}A_{1n}\phi_{1n}(x) =$$

$$\begin{cases} -\gamma_{2p}A'_{2p}\phi_{2p}(x) + \sum_{n=1}^{\infty} \gamma_{2n}A_{2n}\phi_{2n}(x) & , \ 0 < x < b \\ -\gamma_{3p}A'_{3p}\phi_{3p}(x) + \sum_{n=1}^{\infty} \gamma_{3n}A_{3n}\phi_{3n}(x) & , \ b < x < a \end{cases} \qquad (2b)$$

From these relations a set of equations involving the unknown coefficients is derived by making use of the mode orthogonality property. This is done by multiplying (2) by $\phi_{2m}(x)$ and $\phi_{3m}(x)$ and integrating with respect to x from o to b and from b to a, respectively. The results are:

$$\frac{A'_{1p}H_pF_m}{\gamma_{2m}^2 - \gamma_{1p}^2} + \sum_{n=1}^{\infty} \frac{A_{1n}H_nF_m}{\gamma_{2m}^2 - \gamma_{1n}^2} = A'_{2p}\delta_m^p + A_{2m} \qquad (3a)$$

$$\frac{-\gamma_{1p}A'_{1p}H_pF_m}{\gamma_{2m}^2 - \gamma_{1p}^2} + \sum_{n=1}^{\infty} \frac{\gamma_{1n}A_{1n}H_nF_m}{\gamma_{2m}^2 - \gamma_{1n}^2} = -\gamma_{2p}A'_{2p}\delta_m^p + \gamma_{2m}A_{2m} \qquad (3b)$$

$$\frac{A'_{1p}H_pG_m}{\gamma_{3m}^2 - \gamma_{1p}^2} + \sum_{n=1}^{\infty} \frac{A_{1n}H_nG_m}{\gamma_{3m}^2 - \gamma_{1n}^2} = A'_{3p}\delta_m^p + A_{3m} \qquad (3c)$$

$$\frac{-\gamma_{1p}A'_{1p}H_pG_m}{\gamma_{3m}^2 - \gamma_{1p}^2} + \sum_{n=1}^{\infty} \frac{\gamma_{1n}A_{1n}H_nG_m}{\gamma_{3m}^2 - \gamma_{1n}^2} = -\gamma_{3p}A'_{3p}\delta_m^p + \gamma_{3m}A_{3m} \qquad (3d)$$

where F_n, G_n and H_n are parameters determined readily for a given structure (see Appendix B) and δ_m^p is the Kronecker delta function. The above equations are rearranged by eliminating one term on the right hand side to yield

$$\frac{A'_{1p}H_p}{-\gamma_{1p}-\gamma_{2m}}+\sum_{n=1}^{\infty}\frac{A_{1n}H_n}{\gamma_{1n}-\gamma_{2m}}=-2\gamma_{2m}\frac{A_{2m}}{F_m} \qquad (4a)$$

$$\frac{A'_{1p}H_p}{-\gamma_{1p}+\gamma_{2m}}+\sum_{n=1}^{\infty}\frac{A_{1n}H_n}{\gamma_{1n}+\gamma_{2m}}=2\gamma_{2p}\frac{A'_{2p}}{F_p}\delta_m^p \qquad (4b)$$

$$m = 1,2,....$$

$$\frac{A'_{1p}H_p}{-\gamma_{1p}-\gamma_{3m}}+\sum_{n=1}^{\infty}\frac{A_{1n}H_n}{+\gamma_{1n}-\gamma_{3m}}=-2\gamma_{3m}\frac{A_{3m}}{G_m} \qquad (4c)$$

$$\frac{A'_{1p}H_p}{-\gamma_{1p}+\gamma_{3m}}+\sum_{n=1}^{\infty}\frac{A_{1n}H_n}{\gamma_{1n}+\gamma_{3m}}=2\gamma_{3p}\frac{A'_{3p}}{G_p}\delta_m^p \qquad (4d)$$

This infinite set of equations is to be solved simultaneously for the unknown coefficients $\{A_{in}\}$.

An alternative set of equations may also be derived by multiplying the equations (2) by $\phi_{1m}(x)$ and integrating with respect to x from o to a. The resulting equations are:

$$\frac{A'_{2p}F_p}{-\gamma_{2p}+\gamma_{1m}}+\sum_{n=1}^{\infty}\frac{A_{2n}F_n}{\gamma_{2n}+\gamma_{1m}}+\frac{A'_{3p}G_p}{-\gamma_{3p}+\gamma_{1m}}+\sum_{n=1}^{\infty}\frac{A_{3n}G_n}{\gamma_{3n}+\gamma_{1m}}$$

$$=-2\gamma_{1p}\frac{A'_{1p}}{H_p}\delta_m^p \qquad (5a)$$

$$m = 1,2,...$$

$$\frac{A'_{2p}F_p}{-\gamma_{2p}-\gamma_{1m}}+\sum_{n=1}^{\infty}\frac{A_{2n}F_n}{\gamma_{2n}-\gamma_{1m}}+\frac{A'_{3p}G_p}{-\gamma_{3p}-\gamma_{1m}}+\sum_{n=1}^{\infty}\frac{A_{3n}G_n}{\gamma_{3n}-\gamma_{1m}}=2\gamma_{1m}\frac{A_m}{H_m} \qquad (5b)$$

Thus far, the mode-matching formulation has led to two sets of equations, (4) and (5). Since the existence of the layered dielectrics does not affect the edge condition of the septum, the equations are of the same form as that for a bifurcated waveguide described in [8] and the scattering parameters of the junction are obtainable by the residue calculus technique.

If there is only one incident wave coming from region I, i.e., $A'_{2p}=A'_{3p}=0$, (4) becomes

$$\sum_{n=1}^{\infty}\frac{A_{1n}H_n}{\gamma_{1n}-\gamma_{2m}}+\frac{A'_{1p}H_p}{-\gamma_{1p}-\gamma_{2m}}=-2\gamma_{2m}\frac{A_{2m}}{F_m} \qquad (6a)$$

$$m=1,2,3,\ldots$$

$$\sum_{n=1}^{\infty}\frac{A_{1n}H_n}{\gamma_{1n}+\gamma_{2m}}+\frac{A'_{1p}H_p}{-\gamma_{1p}+\gamma_{2m}}=0 \qquad (6b)$$

$$\sum_{n=1}^{\infty}\frac{A_{1n}H_n}{\gamma_{1n}-\gamma_{3m}}+\frac{A'_{1p}H_p}{-\gamma_{1p}-\gamma_{3m}}=-2\gamma_{3m}\frac{A_{3m}}{G_m} \qquad (6c)$$

$$\sum_{n=1}^{\infty}\frac{A_{1n}H_n}{\gamma_{1n}+\gamma_{3m}}+\frac{A'_{1p}H_p}{-\gamma_{1p}+\gamma_{3m}}=0 \qquad (6d)$$

Consider the integrals

$$\frac{1}{2\pi j}\oint_C\frac{f(w)}{w-\gamma_{2m}}dw \quad , \quad \text{and} \quad \frac{1}{2\pi j}\oint_C\frac{f(w)}{w+\gamma_{2m}}dw, \qquad (7)$$

$$\frac{1}{2\pi j}\oint_C \frac{f(w)}{w - \gamma_{3m}}\,dw \quad , \quad \text{and} \quad \frac{1}{2\pi j}\oint_C \frac{f(w)}{w + \gamma_{3m}}\,dw \qquad (7)$$

where the contour C is an infinitely large circle in the complex w-plane, traversed in the counterclockwise direction. Let the function f(w) satisfy the following conditions:

1. f(w) is an analytic function of w except for simple poles at $w = \gamma_{1n}$, $n = 1,2,3,\ldots$ and at $w = -\gamma_{1p}$.
2. f(w) has simple zeroes at $w = -\gamma_{2m}$, and $w = -\gamma_{3m}$, $m = 1,2,3\ldots$
3. The residue of f(w) at $w = -\gamma_{1p}$ is equal to $A'_{1p}H_p$.
4. f(w) has algebraic behavior at infinity. Specifically, $f(w) = O(w^{-3/2})$.

In view of condition 4, the integrands in (7) are $O(w^{-5/2})$ on the contour C; consequently, these integrals are equal to zero. Expressing the integrals in terms of series of residues on f(w) and equating the results to zero we have

$$\sum_{n=1}^{\infty} \frac{\text{Res}f(\gamma_{1n})}{\gamma_{1n} - \gamma_{2m}} + \frac{A'_{1p}H_p}{-\gamma_{1p} - \gamma_{2m}} + f(\gamma_{2m}) = 0 \qquad (8a)$$

$$\sum_{n=1}^{\infty} \frac{\text{Res}f(\gamma_{1n})}{\gamma_{1n} + \gamma_{2m}} + \frac{A'_{1p}H_p}{-\gamma_{1p} + \gamma_{2m}} = 0 \qquad (8b)$$

$$\sum_{n=1}^{\infty} \frac{\text{Res}f(\gamma_{1n})}{\gamma_{1n} - \gamma_{3m}} + \frac{A'_{1p}H_p}{-\gamma_{1p} - \gamma_{3m}} + f(\gamma_{3m}) = 0 \qquad (8c)$$

$$\sum_{n=1}^{\infty} \frac{\text{Res}f(\gamma_{1n})}{\gamma_{1n} + \gamma_{3m}} + \frac{A'_{1p}H_p}{-\gamma_{1p} + \gamma_{3m}} = 0 \qquad (8d)$$

for m = 1,2,3,..., where the condition 3 of f(w), $\mathrm{Resf}(-\gamma_{1p}) = A_1 H_{1p}$, has been applied. A comparison of (I-8) and (I-6) immediately shows that,

$$A_{1n} = \mathrm{Resf}(\gamma_{1n})/H_n \qquad (9a)$$

$$A_{2m} = F_m f(\gamma_{2m})/(2\gamma_{2m}) \qquad (9b)$$

$$A_{3m} = G_m f(\gamma_{3m})/(2\gamma_{3m}) \qquad (9c)$$

The unknowns $\{A_{in}\}$ are readily determined if f(w) is known.

At this stage the reason for enforcing the four conditions on f(w) becomes obvious. The pole structure given in condition 1 was chosen to make the residue series involving $\{\gamma_{in}\}$ identical to the left hand side of (6), while the assigned locations of the zeroes of f(w) in condition 2 ensure that no contribution comes from the poles at $w = -\gamma_{2m}$ and $-\gamma_{3m}$ in the contour integrals. Condition 3 brings the dependence of the incident wave into the final solution and may, therefore, be regarded as a normalization of f(w). Condition 4 not only ensures that the contour integrals are zero, but also allows unique determination of the solution by means of the specific large-argument asymptotic behavior of f(w). Condition 4 is related to the edge condition [11]. This point will become clear when f(w) is to be constructed for solutions.

The construction of f(w) is the key step in the residue-calculus method. First, the zero and pole conditions in 1 and 2

can be satisfied by assuming the general form for f(w) to be

$$f(w) = f_o(w) \frac{1}{(1 + w/\gamma_{1p})} \prod_{n=1}^{\infty} \frac{(1+w/\gamma_{2n})(1+w/\gamma_{3n})}{(1 - w/\gamma_{1n})} \qquad (10)$$

where $f_o(w)$ is an entire function of w that is to be determined from the remaining conditions 3 and 4. To this end, a study of the asymptotic behavior of the infinite product in (10) [8] shows that, as $|w| \to \infty$,

$$f(w) \sim h_o(w) f_o(w)\ w^{-3/2}\ e^{-Lw} \qquad (11a)$$

where

$$L = \frac{b}{\pi} \ln\left(\frac{a}{b}\right) + \frac{c}{\pi} \ln\left(\frac{a}{c}\right) \qquad (11b)$$

and $h_o(w)$ is bounded as $|w| \to \infty$. Since condition 4 requires that $f(w) = 0(w^{-3/2})$ as $|w| \to \infty$, it is satisfied by choosing

$$f_o(w) = h\ e^{Lw} \qquad (12)$$

The only remaining unknown constant h can be determined by using condition 3. Incorporating this in (10) we obtain the final form for f(w):

$$f(w) = A'_{1p} H_p\ e^{L(w + \gamma_{1p})} \frac{1}{\gamma_{1p} + w} \prod_{n=1}^{\infty} \frac{(\gamma_{1n}+\gamma_{1p})(\gamma_{2n}+w)(\gamma_{3n}+w)}{(\gamma_{1n}-w)(\gamma_{2n}-\gamma_{1p})(\gamma_{3n}-\gamma_{1p})} \qquad (13)$$

The desired solutions for $\{A_{in}\}$ are derived by employing (13) in (9). From these solutions, expressions for the scattering parameters $S_{i1}(m,p) = A_{im}/A'_{1p}$ are obtained:

$$S_{11}(m,p) = -\frac{H_p}{H_m} e^{L(\gamma_{1m} + \gamma_{1p})} \frac{(\gamma_{1m} - \gamma_{1m})}{(\gamma_{1p} + \gamma_{1m})} \cdot$$

(14a)

$$\prod_{n=1}^{\infty} \frac{(\gamma_{1n} + \gamma_{1p})\ (\gamma_{2n} + \gamma_{1m})\ (\gamma_{3n} + \gamma_{1m})}{(\gamma_{1n} - \gamma_{1m})\ (\gamma_{2n} - \gamma_{1p})\ (\gamma_{3n} - \gamma_{1p})} -$$

$$S_{21}(m,p) = \frac{F_m H_p}{2\gamma_{2m}} e^{L(\gamma_{2m} + \gamma_{1p})} \frac{1}{(\gamma_{1p} + \gamma_{2m})} \cdot$$

(14b)

$$\prod_{n=1}^{\infty} \frac{(\gamma_{1n} + \gamma_{1p})\ (\gamma_{2n} + \gamma_{2m})\ (\gamma_{3n} + \gamma_{2m})}{(\gamma_{1n} - \gamma_{2m})\ (\gamma_{2n} - \gamma_{1p})\ (\gamma_{3n} - \gamma_{1p})}$$

$$S_{31}(m,p) = \frac{G_m H_p}{2\gamma_{3m}} e^{L(\gamma_{3m} + \gamma_{1p})} \frac{1}{(\gamma_{1p} + \gamma_{3m})} \cdot$$

(14c)

$$\prod_{n=1}^{\infty} \frac{(\gamma_{1n} + \gamma_{1p})\ (\gamma_{2n} + \gamma_{3m})\ (\gamma_{3n} + \gamma_{3m})}{(\gamma_{1n} - \gamma_{3m})\ (\gamma_{2n} - \gamma_{1p})\ (\gamma_{3n} - \gamma_{1p})}$$

In a similar manner, assumption of a single incident wave $A'_{2p}\phi_{2p}(x)$ or $A'_{3p}\phi_{3p}(x)$ in equation (4) and repetition of the procedure yield the expressions for $S_{i2}(m,p)$ or $S_{i3}(m,p)$, respectively. They are summarized in the following:

$$S_{12}(m,p) = \frac{2\gamma_{2p}}{H_m F_p} e^{L(\gamma_{2p} + \gamma_{1m})} \frac{(\gamma_{1m} - \gamma_{1m})\ (\gamma_{2p} - \gamma_{2p})}{(\gamma_{2p} - \gamma_{1m})} \cdot$$

(14d)

$$\prod_{n=1}^{\infty} \frac{(\gamma_{1n} + \gamma_{2p})\ (\gamma_{2n} + \gamma_{1m})\ (\gamma_{3n} + \gamma_{1m})}{(\gamma_{1n} - \gamma_{1m})\ (\gamma_{2n} - \gamma_{2p})\ (\gamma_{3n} - \gamma_{2p})}$$

$$S_{22}(m,p) = -\frac{\gamma_{2p}}{\gamma_{2m}} \frac{F_m}{F_p} e^{L(\gamma_{2p} + \gamma_{2m})} \frac{(\gamma_{2p} - \gamma_{2p})}{(\gamma_{2p} + \gamma_{2m})} \cdot$$

(14e)

$$\prod_{n=1}^{\infty} \frac{(\gamma_{1n} + \gamma_{2p})\ (\gamma_{2n} + \gamma_{2m})\ (\gamma_{3n} + \gamma_{2m})}{(\gamma_{1n} - \gamma_{2m})\ (\gamma_{2n} - \gamma_{2p})\ (\gamma_{3n} - \gamma_{2p})}$$

$$S_{32}(m,p) = -\frac{\gamma_{2p}}{\gamma_{3m}} \frac{G_m}{F_p} e^{L(\gamma_{2p} + \gamma_{3m})} \frac{(\gamma_{2p} - \gamma_{2p})}{(\gamma_{2p} + \gamma_{3m})} \cdot$$

(14f)

$$\prod_{n=1}^{\infty} \frac{(\gamma_{1n} + \gamma_{2p})\ (\gamma_{2n} + \gamma_{3m})\ (\gamma_{3n} + \gamma_{3m})}{(\gamma_{1n} - \gamma_{3m})\ (\gamma_{2n} - \gamma_{2p})\ (\gamma_{3n} - \gamma_{2p})}$$

$$S_{13}(m,p) = \frac{2\gamma_{3p}}{H_n G_p} e^{L(\gamma_{3p} + \gamma_{1m})} \frac{(\gamma_{1m} - \gamma_{1m})\ (\gamma_{3p} - \gamma_{3p})}{(\gamma_{3p} - \gamma_{1m})} \cdot$$

(14g)

$$\prod_{n=1}^{\infty} \frac{(\gamma_{1n} + \gamma_{3p})\ (\gamma_{2n} + \gamma_{1m})\ (\gamma_{3n} + \gamma_{1m})}{(\gamma_{1n} - \gamma_{1m})\ (\gamma_{2n} - \gamma_{3p})\ (\gamma_{3n} - \gamma_{3p})}$$

$$S_{23}(m,p) = -\frac{\gamma_{3p}}{\gamma_{2m}} \frac{F_m}{G_p} e^{L(\gamma_{3p} + \gamma_{2m})} \frac{(\gamma_{3p} - \gamma_{3p})}{(\gamma_{3p} + \gamma_{2m})} \cdot$$

(14h)

$$\prod_{n=1}^{\infty} \frac{(\gamma_{1n} + \gamma_{3p})\ (\gamma_{2n} + \gamma_{2m})\ (\gamma_{3n} + \gamma_{2m})}{(\gamma_{1n} - \gamma_{2m})\ (\gamma_{2n} - \gamma_{3p})\ (\gamma_{3n} - \gamma_{3p})}$$

$$S_{33}(m,p) = -\frac{\gamma_{3p}}{\gamma_{3m}} \frac{G_m}{G_p} e^{L(\gamma_{3p} + \gamma_{3m})} \frac{(\gamma_{3p} - \gamma_{3p})}{(\gamma_{3p} + \gamma_{3m})} \cdot$$

(14i)

$$\prod_{n=1}^{\infty} \frac{(\gamma_{1n} + \gamma_{3p})\ (\gamma_{2n} + \gamma_{3m})\ (\gamma_{3n} + \gamma_{3m})}{(\gamma_{1n} - \gamma_{3m})\ (\gamma_{2n} - \gamma_{3p})\ (\gamma_{3n} - \gamma_{3p})}$$

Notice that in the preceding equation (14) the expressions $(\gamma_{1m} - \gamma_{1m})$, $(\gamma_{2p} - \gamma_{2p})$, and $(\gamma_{3p} - \gamma_{3p})$ are introduced to cancel the corresponding poles in the infinite products. The notation $S_{ij}(m,p)$ stands for the scattering coefficient of the m-th order mode in region i due to the p-th order mode excitation incident from region j. This set of equations is thus valid for any mode.

An alternative set of solutions for $S_{ij}(m,p)$ can be obtained by solving the set of equations in (5). The results provide a valuable checking tool in numerical calculations. They are, therefore, summarized in Appendix C.

B. Step 2 -- Finite-Length Septum

In step 1, we have characterized the single junction by means of a three-port scattering matrix that has nine elements. Each of the elements is also a matrix of infinite dimensions that corresponds to the infinite number of eigenmodes. With the knowledge of the scattering parameters for a single junction, the generalized scattering matrix technique is applied to obtain a two-port scattering matrix as shown in Fig. 4. Suppose now that the TE-type wave from region I is incident upon junction A. At this junction, fields are partly reflected back into region I and partly transmitted into regions II and III. After traveling a distance d, part of the wave transmitted into regions II and III is reflected back and part is transmitted into region I' at junction B. This

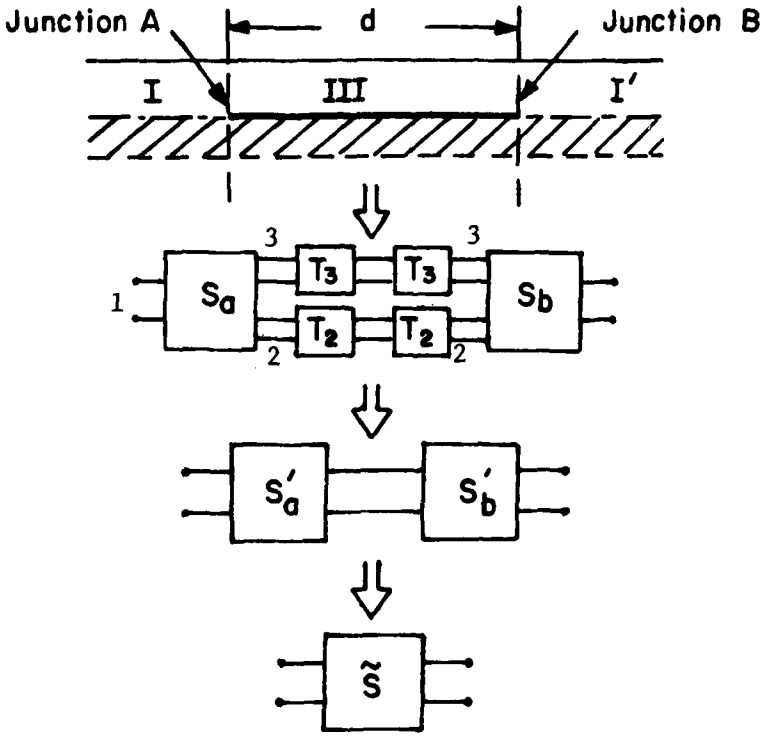

Fig. 4. Derivation of S parameters for a finite-length septum.

process continues until the intensity of the reflected wave dies out. The multiple-reflection phenomenon between junctions A and B is implied in a matrix manipulation which yields the scattering matrix for a finite length septum.

In Fig. 4, S_a and S_b represent the scattering matrices for isolated junctions A and B (i.e., for semi-infinite septums), respectively. From equation (14) we obtain the value of the elements in both matrices. Since the characteristics of these two junctions are essentially the same except for the opposite orientation, if we define the port numbers of the networks as shown in Fig. 4, we have

$$S_b = S_a = S \qquad (15)$$

where S is the scattering matrix defined by (14).
We now define the transmission matrix

$$T = \begin{bmatrix} [I] & [0] & [0] \\ [0] & [T_2] & [0] \\ [0] & [0] & [T_3] \end{bmatrix} \qquad (16)$$

where [I] and [0] are the identity matrix and the zero matrix, respectively; $[T_2]$ and $[T_3]$ are diagonal matrices of infinite size, whose diagonal elements are $T_{2ii} = e^{-\gamma_{2i} d/2}$ and $T_{3ii} = e^{-\gamma_{3i} d/2}$ for i from 1 to ∞, respectively. In effect, $[T_2]$ and $[T_3]$ represent the wave propagating (for propagation modes) or attenuating (for evanescent modes) for a distance of d/2 in guided regions II and III, respectively. The combination of the transmission matrix along with S_a and S_b results in S_a' and S_b':

$$S'_a = S'_b = TST = S' \qquad (17)$$

A further combination of S'_a and S'_b then yields the composite scattering matrix $\tilde{S}$

$$\tilde{S} = \begin{bmatrix} \tilde{S}_{11} & \tilde{S}_{12} \\ \tilde{S}_{21} & \tilde{S}_{22} \end{bmatrix} = \begin{bmatrix} \underline{S}_{12} & \underline{S}_{13} \\ S'_{12} & S'_{13} \end{bmatrix} \begin{bmatrix} I-\underline{S}_{22} & -\underline{S}_{23} \\ -\underline{S}_{32} & I-\underline{S}_{33} \end{bmatrix}^{-1} \begin{bmatrix} S'_{21} & \underline{S}_{21} \\ S'_{31} & \underline{S}_{31} \end{bmatrix} + \begin{bmatrix} S'_{11} & \underline{S}_{11} \\ 0 & S'_{11} \end{bmatrix} \qquad (18)$$

where

$$\underline{S}_{ij} = \sum_{k=2}^{3} S'_{ik} S'_{kj} \qquad i,j = 1,2,3$$

that represents the septum of length d, viewed from I at z = 0 and from I' at z = d.

C. Step 3 -- Filter Structure

For the final step of the analysis, several finite length septa are cascaded with appropriate separations to form a filter circuit. This is done by using the same techniques used in step 2 described above. The procedure depicted in Fig. 5 shows the cascading of two septa represented by $\tilde{S}_a$ and $\tilde{S}_b$. The comination of $\tilde{S}_a$ and the transmission matrix T_1 results in matrix $\tilde{S}'_a$ which is further combined with $\tilde{S}_b$ to yield $\bar{S}$, the total scattering matrix of two septa with a separation of ℓ.

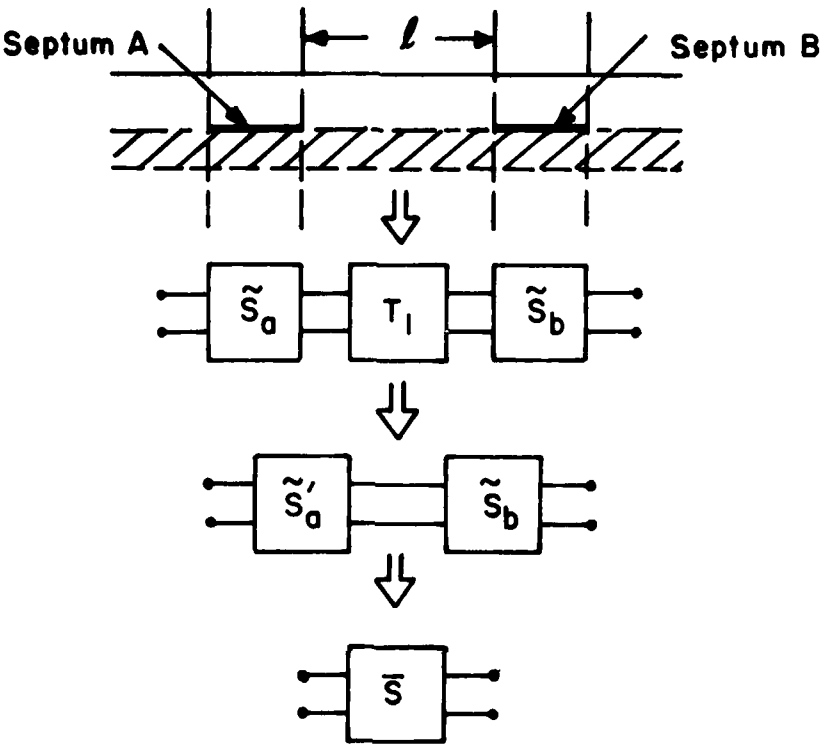

Fig. 5. Derivation of S parameters for cascading septa.

$$\bar{S} = \begin{bmatrix} S'_{a12}S_{b11} \\ S_{b21} \end{bmatrix} \left[I - S'_{a22}S_{b11} \right]^{-1} \begin{bmatrix} S'_{a21} & S'_{a22}S_{b12} \end{bmatrix} + \begin{bmatrix} S'_{a11} & S'_{a12}S_{b12} \\ 0 & S_{b22} \end{bmatrix} \tag{19}$$

This process is repeated to obtain the scattering parameters of a filter structure consisting of any number of septa.

D. Numerical Considerations

Based on the above analysis, a computer program is developed to calculate the total scattering parameters for a filter structure with given design parameters. This analysis program is to be used later in an optimization routine. Since the scattering parameters of the semi-infinite septum depend only on the waveguide size and dielectric properties that are constant factors in a design, the calculations in step 1 need to be done only once at each frequency point. These calculations may be regarded as pre-calculations to the optimization routine; therefore, the optimization procedure requires only the calculations in steps 2 and 3.

Although the analysis is formally exact, in practice the infinite products in (14) and the infinite dimensions of the elements in the scattering matrices need to be truncated. To guarantee the reliability of numerical results, the degree of convergence in the numerical calculations is studied. The numerical results show that the infinite products in (14) converge very fast. Table 1

Table 1. Scattering parameters of semi-infinite septum.
Bilateral structure (b/a = .254/7.112, ε_r = 2.22)

	S_{11} (Amplitude, Phase Angle)		S_{21} (Amplitude, Phase Angle)	
N	a/λ= 7.112/12.	7.112/7.5	7.112/12.	7.112/7.5
1	(1.0,2.39285)	(1.0,1.05275)	(.123349,1.19643)	(.274516,.526374)
2	(1.0,2.53385)	(1.0,1.44099)	(.117937,1.26693)	(.266715,.720497)
3	(1.0,2.61077)	(1.0,1.63158)	(.118430,1.30538)	(.263645,.815790)
10	(1.0,2.65991)	(1.0,1.74908)	(.117924,1.32995)	(.262418,.874539)
40	(1.0,2.68554)	(1.0,1.80955)	(.117790,1.34277)	(.262138,.904775)
100	(1.0,2.69077)	(1.0,1.82185)	(.117771,1.34538)	(.262097,.910923)
200	(1.0,2.69252)	(1.0,1.82592)	(.117766,1.34626)	(.262084,.912981)
300	(1.0,2.69310)	(1.0,1.82734)	(.117764,1.34655)	(.262080,.913668)
400	(1.0,2.69339)	(1.0,1.82802)	(.117763,1.34670)	(.262078,.914012)
500	(1.0,2.69359)	(1.0,1.82844)	(.117762,1.34785)	(.262077,.914218)

gives two typical calculations of $S_{11}(1,1)$ and $S_{21}(1,1)$ as the number of terms in the product is increased. Although fairly accurate results may be obtained by using the first few terms (≤ 10), at least 300 terms are required to achieve an accuracy of 0.1 percent. The calculation of the products here is efficient since only readily known propagation constants are involved.

For most applications, the fundamental mode is below cutoff in the narrow waveguide section (regions II and III) and all of the higher order modes are evanescent in the wide waveguide (region 1). Therefore, only the first few accessible modes [12] are essentially responsible for the coupling between resonators. For most cases, only two or three modes are required to describe accurate scattering behavior. Typical examples of $S_{11}(1,1)$ for septa of lengths d = 1 mm and 5 mm, calculated using up to 5 modes, are shown in Table 2. It is clear that more modes need to be used for a short septum at a higher frequency. Notice that the number of modes considered here indicates the dimensions of the matrices to be manipulated in steps 2 and 3. The calculation includes a number of complex matrix multiplications and inversions. This analysis is efficient mainly due to the fact that the matrix size is kept small.

Table 2. Reflection coefficients of finite-length septum.
Bilateral structure (b/a = .254/7.112, ε_r = 2.22)

	f = 30 GHz		f = 40 GHz	
M	d(mm) = 1	5	1	5
1	(.930870,2.416296)	(.999657,2.438459)	(.809566,1.968796)	(.990251,1.835966)
2	(.924827,2.411486)	(.999657,2.438458)	(.797303,1.967360)	(.990246,1.835966)
3	(.923936,2.410614)	(.999657,2.438458)	(.795527,1.966800)	(.990246,1.835966)
4	(.923755,2.410420)	(.999657,2.438458)	(.795168,1.966653)	(.990246,1.835966)
5	(.923712,2.410371)	(.999657,2.438458)	(.795082,1.966613)	(.990246,1.835966)

E. Optimization

The analysis algorithm is then used by an optimization computer program [13] that varies the input parameters until a desired value of the insertion loss for a given bandwidth is obtained. This is done by defining an error (objective) function $F(\bar{x})$ as follows:

$$F(\bar{x}) = \sum_{N_s} \left(\frac{L_s}{|S_{21}|} \right)^2 + \sum_{N_p} \left(\frac{|S_{21}|}{L_s} \right)^2 \qquad (20)$$

where N_s and N_p are the number of frequency sampling points in the stopband and passband, respectively; L_s and L_p are the minimum stopband and maximum passband attenuation levels, respectively; $|S_{21}|$ is the calculated value of the filter attenuation. For a given thickness of the dielectric, the parameters $\bar{x}$ to be optimized are the septum lengths and resonator lengths.

To prevent the program from approaching non-realizable or non-physical results, upper and lower bounds of each parameter are specified

$$x_{\ell i} < x_i < x_{ui} \qquad (21)$$

The constrained parameters are then reduced into essentially unconstrained ones by the transformation [14]

$$x_i = x_{\ell i} + \frac{1}{\pi} (x_{ui} - x_{\ell i}) \cot^{-1} x'_i \qquad (22)$$

where $-\infty < x_i' < \infty$ but only solutions within the range

$$0 < \cot^{-1} x_i' < \pi \qquad (23)$$

are allowed. This transformation has a penalizing effect upon the parameters in the vicinity of the upper and lower bounds.

For the optimization procedure, the first two modes in each subregion are considered; the final design values are calculated with three modes. The total computing time for optimizing a five resonator filter was about 2 minutes on a CDC Dual Cyber 170/750.

F. Experiments

In an earlier publication [15], it has been pointed out that the Q-factor in insulated finlines is inferior to that of bilateral finlines. Therefore, the design of filters using insulated finlines will not be considered in this study. Further, the E-plane circuits usually employ a relatively thick metal sheet; these circuits will be discussed in the next chapter.

In the present study, bandpass filters in bilateral and unilateral finline configurations are designed and fabricated on RT/Duroid substrate. Some typical designs for Ka-band applications are shown in Figures 6 and 8. Notice that the resonators are very weakly coupled by wide septa. In such cases, the septum cannot be represented by simple shunt-inductance equivalent circuits. Instead, it has to be represented by an equivalent T network [1].

Since the equivalent circuits are useful in conventional circuit design and are helpful for good initial guesses in the optimization procedure, this topic is discussed briefly in Appendix D.

The five-resonator filter design in Fig. 6 is a bilateral structure in which the hatched portion indicates metal on both sides of the substrate. The center frequency is 38.85 GHz; the 0.1 dB ripple bandwidth is 1.1 GHz; and the skirt selectivity is -40 dB at 500 MHz away from either edge of the passband. Measured characteristics of this filter are shown in Figure 7. Computed responses are also plotted for comparison. Shapes of the calculated and measured response curves agree extremely well. Measured insertion loss in the passband is less than 1.3 dB, of which 0.3 dB is associated with the test fixture. The measured center frequency is shifted to the lower side by about 170 MHz, which is less than 0.5% of the center frequency.

Fig. 8 shows a photograph of a three-resonator bilateral finline filter printed on a 10-mil thick RT/Duroid substrate. The design specifications for this fitler were the same as those for the last one except for a decreased skirt selectivity of -20 dB. The measured results in Fig. 9 show that the insertion loss is less than 0.8 dB in the passband, including the fixture loss. The calculated and measured frequency responses again agree well; however, the measured center frequency is shifted down by about 300 MHz.

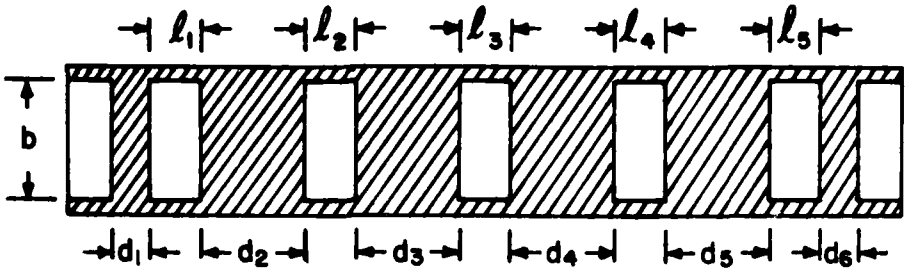

Resonator Length:

$\ell_1 = \ell_5 = 2.6594$ mm

$\ell_2 = \ell_4 = 2.6205$ mm

$\ell_3 = 2.6195$ mm

Septum Length:

$d_1 = d_6 = 1.6749$ mm

$d_2 = d_5 = 5.2786$ mm

$d_3 = d_4 = 5.8584$ mm

Substrate: RT/Duroid

$\varepsilon_r = 2.2$

Thickness = .254 mm

Waveguide: Height b = 3.556 mm

Width a = 7.112 mm

Fig. 6. Design example of 5-resonator bilateral filter.

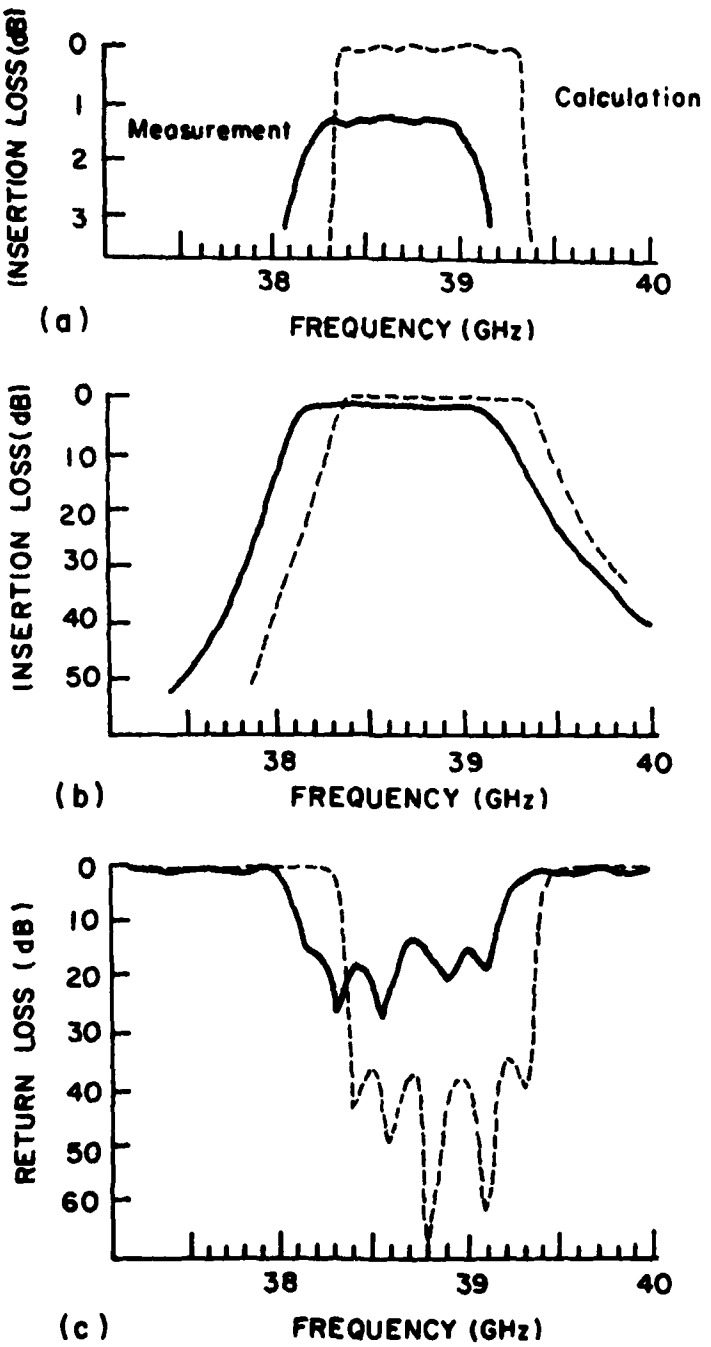

Fig. 7. Frequency response of the filter in Fig. 6. (a) Expanded view of insertion loss, (b) Insertion loss characteristics, (c) Return loss characteristics.

Three-Resonator Bilateral Finline Filter

Resonator Length:

$\ell_1 = \ell_3 = 2.6559$ mm

$\ell_2 = 2.6187$ mm

Septum Width:

$d_1 = d_4 = 1.7230$ mm

$d_2 = d_3 = 5.3628$ mm

Fig. 8. Three-resonator Ka-band bilateral filter.

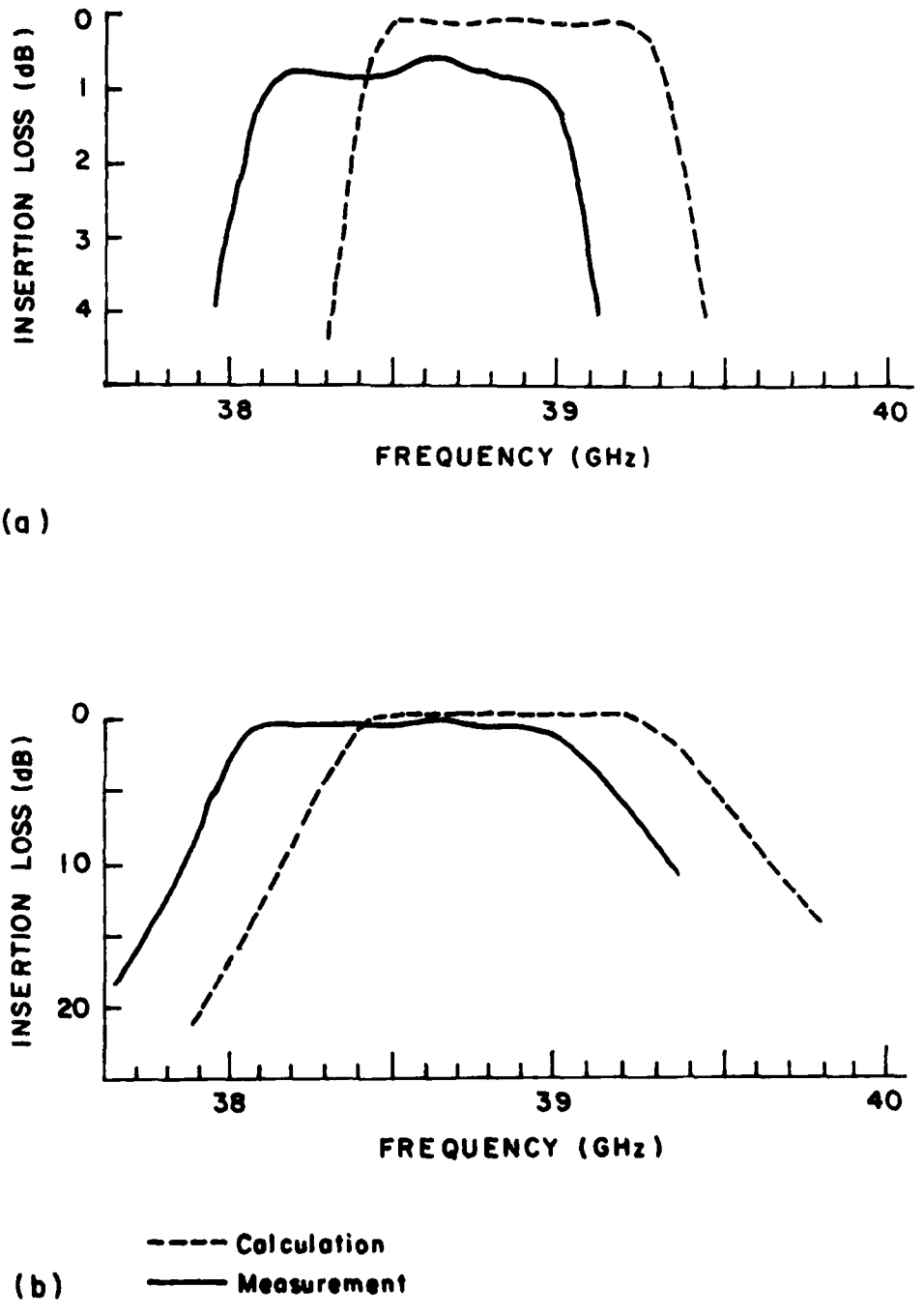

Fig. 9. Frequency response of the filter in Fig. 8. (a) Expanded view of insertion loss, (b) Insertion loss characteristics.

Bandpass filters have also been developed in unilateral finline configurations. A typical design for a three-resonator filter has the following specifications and dimensions:

Resonator lengths: $\ell_1 = \ell_3 = 2.1568$ mm; $\ell_2 = 2.0879$ mm

Septum widths: $d_1 = d_4 = 2.3325$ mm; $d_2 = d_3 = 6.8718$ mm

Passband: 39.0 $\sim$ 39.7 GHz, Chebyshev response with 0.1 dB ripple

Skirt selectivity: -20 dB at 500 MHz away from passband edge

The measured results in Fig. 10 show about 2 dB insertion loss in the passband and about 200 MHz downward shift for the center frequency.

In the experiments performed, the measured center frequencies are always lower than the calculated values. The deviations range from 170 MHz to 300 MHz. One cause of this shift is that the filter structure assembled is different from the one analyzed. The assembled structure has 10-mil-deep grooves machined into the top and bottom walls to support the substrate in the waveguide. An experimental study on this effect shows that within the quarter-wavelength range, the deeper the groove is made, the more the center frequency will shift down. Another possible source of the discrepancy is the finite thickness of the metal fin. The thickness effect is minor at this frequency since the thickness of the copper cladding on the substrate is about 0.5 mil. However,

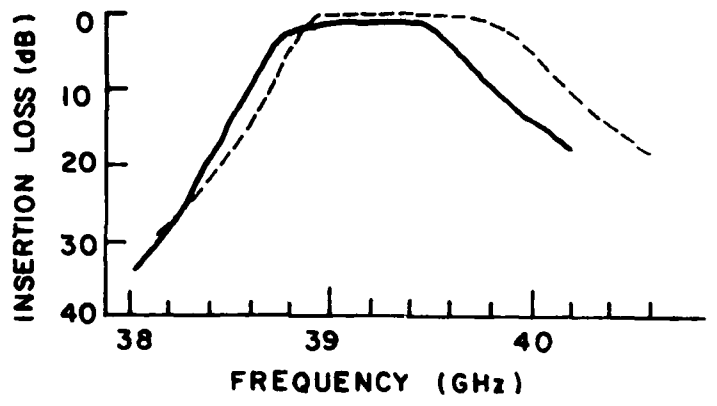

(a)

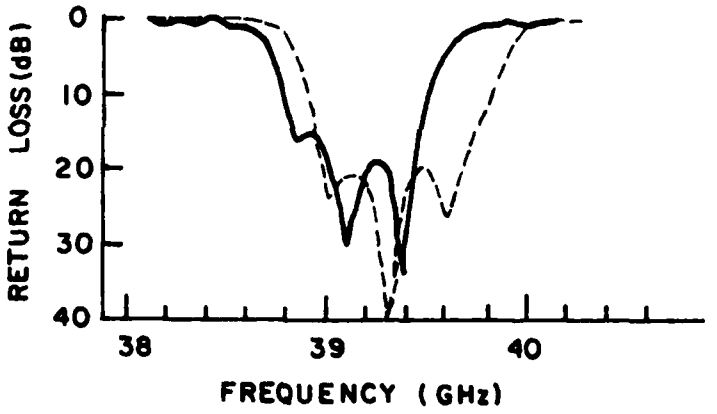

(b)

Fig. 10. Frequency response of a 3-resonator unilateral filter. (a) Insertion loss characteristics, (b) Return loss characteristics.

it will become an important factor for higher frequency applications, such as W-band circuits. These effects are discussed in the next chapter.

From the experiments, it has been observed that the insertion loss of a unilateral filter is always greater than that of a bilateral filter for similar design specifications. One possible explanation is that the dielectric loss of the unilateral filter is greater, while the conductor loss is about the same in both cases. In the case of bilateral finlines, little energy can penetrate into the very narrow space between the strips. Therefore, the energy is mainly coupled through the wider empty waveguide section. In the unilateral case, the energy is coupled about evenly through the empty guide and the partially dielectric-filled guide region. Obviously, more dielectric loss is encountered in this case. By the same reasoning we can surmise that the conductor loss is about the same for both cases. Although the bilateral structure has copper cladding on both sides of the substrate, there is essentially no current flowing on the inner surface facing the dielectric. It is thus equivalent to a conducting strip with current flowing on the outer surface of both sides as in the unilateral case. Of course, these statements are strictly conjectural; further study is needed to verify them. This conjecture would also be applicable to the case of insulated finlines versus bilateral finlines.

Another point worth mentioning is the sensitivity of the filter structure to mechanical tolerances. Calculations show that for both cases, the center frequency shifts about 100 MHz if the fabrication error in resonator length is 1 mil. Also, if the dielectric substrate is shifted in the broadwall direction (x-direction) from its centered position, the filter's center frequency falls. This effect is much more noticeable with the unilateral structure. Therefore, the bilateral structure shows more promise from a constructional viewpoint.

III. FILTERS WITH SEPTA OF FINITE THICKNESS

In the previous chapter, we have introduced a design procedure for a class of E-plane waveguide filters. The metal septa used in the circuits, either stand-alone or printed on a substrate, were considered to be infinitesimally thin. This assumption is applicable only when the thickness of the septa is small compared to the wavelength, typically less than 0.3%. When the purely metallic sheet is used, or when the operating frequency is high, this criterion is difficult to satisfy, and the thickness effect must be considered in the analysis for an accurate design.

In this chapter, the design procedure is modified to take into account the thickness of the metal sheets. To this end, step 1 of the previous analysis is replaced by the analysis of a semi-infinite septum of finite thickness. The rest of the design procedure is kept unchanged.

A. Finite-Thickness Septum

Fig. 11a shows the generalized structure to be analyzed, similar to that in Fig. 3 except for the septum of thickness t. Again the excitation field is assumed to be of TE_{po} type. Despite the modal expansions for the fields on either side of the interface z = 0, matching of the transverse components does not lead to a set of equations of the form solvable by the residue-calculus technique. However, the modal nature of the fields in the three regions suggests description of the junction in terms of generalized scattering matrices. The scattering matrices may be derived via the multiple-reflection method for a suitable auxiliary geometry.

The auxiliary geometry appropriate for the thick-septum junction is that of Fig. 11b. The conducting wall due to the thick septum is recessed into region III and two additional regions IV and V are created for convenience of analysis. The original structure can be recovered by reducing both δ_1 and δ_2 to zero. Notice that in this new structure, the characteristics of junctions at z = 0 (junction A) and $z = \delta_1$ (junction B) are essentially the same as that of the thin-septum junction whose exact scattering matrix description was given in the previous chapter. Let the scattering matrices for the junction A have the subscript a, i.e., S_{aij} (i,j = 1,2,4); and let those for the junction B have the subscript b, i.e., S_{bij} (i,j = 4,5,3). The scattering matrices for the composite junction, S_{ij} (i,j = 1,2,3), will have no subscript. Consideration of the multiple-reflection phenomena and reduction of

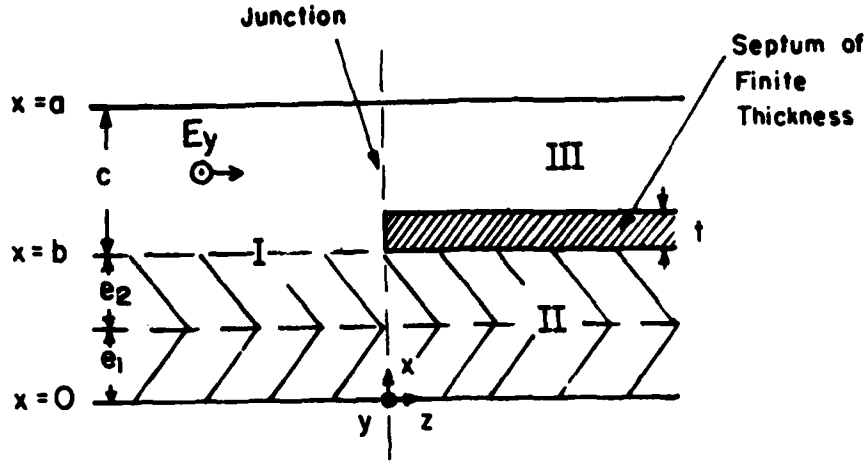

(a)

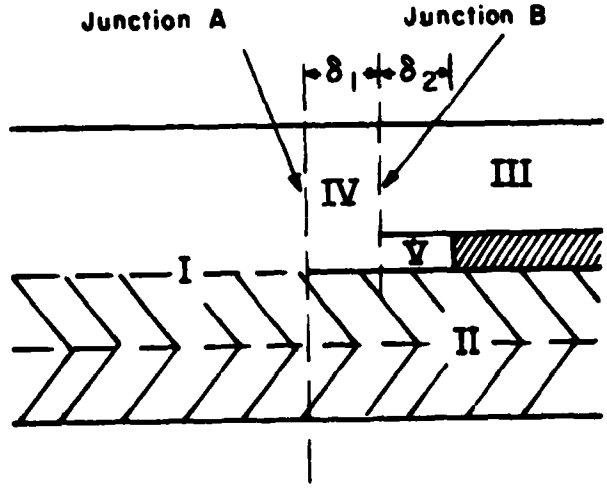

(b)

Fig. 11. Semi-infinite septum of finite thickness. (a) Geometry, (b) Auxiliary structure.

δ_1, δ_2 to zero yields the following representations for the composite scattering matrices:

$$S_{11} = S_{a11} + S_{a14}[I - S'_{b44}S_{a44}]^{-1}S'_{b44}S_{a41} \quad (24a)$$

$$S_{12} = S_{a12} + S_{a14}[I - S'_{b44}S_{a44}]^{-1}S'_{b44}S_{a42} \quad (24b)$$

$$S_{13} = S_{a14}[I - S'_{b44}S_{a44}]^{-1}S'_{b43} \quad (24c)$$

$$S_{21} = S_{a21} + S_{a24}[I - S'_{b44}S_{a44}]^{-1}S'_{b44}S_{a41} \quad (24d)$$

$$S_{22} = S_{a22} + S_{a24}[I - S'_{b44}S_{a44}]^{-1}S'_{b44}S_{a42} \quad (24e)$$

$$S_{23} = S_{24}[I - S'_{b44}S_{a44}]^{-1}S'_{b43} \quad (24f)$$

$$S_{31} = S'_{b34}[I - S_{a44}S'_{b44}]^{-1}S_{a41} \quad (24g)$$

$$S_{32} = S'_{b34}[I - S_{a44}S'_{b44}]^{-1}S_{a42} \quad (24h)$$

$$S_{33} = S'_{b34}[I - S_{a44}S'_{b44}]^{-1}S_{a44}S'_{b43} \quad (24i)$$

where

$$\begin{bmatrix} S'_{b44} & S'_{b43} \\ S'_{b34} & S'_{b33} \end{bmatrix} = \begin{bmatrix} S_{b44} & S_{b43} \\ S_{b34} & S_{b33} \end{bmatrix} - \begin{bmatrix} S_{b45} \\ S_{b35} \end{bmatrix} \left[I + S_{b55}\right]^{-1} \begin{bmatrix} S_{b54} & S_{b53} \end{bmatrix}$$

B. Numerical Considerations

The computation of equation (24) involves a number of matrix inversions and multiplications. The computation time can be significantly reduced by truncating the scattering matrices at the smallest size that yields suitably accurate results. A convergence study shows that for most of the cases only 3 x 3 matrices are required. Some typical examples are shown in Tables 3 and 4 where the dominant scattering parameters of the junction created by a finite-thickness septum are calculated using matrices of sizes ranging from 1 x 1 to 6 x 6. It is clear that in this case a 2 x 2 matrix calculation yields results accurate to the third digit.

C. Thickness Effect

From a physical point of view, the larger the scattering area of an obstacle, the more energy is reflected. However, in a bifurcated waveguide, the change in the scattering area (i.e., the thickness of the septum) does not affect the amplitude of the reflection coefficient since all of the energy is reflected no matter how thin the septum is. It is the phase angle of the reflection coefficient that is affected by the change in thickness. The computed phase angle for a septum located at the center of the waveguide is shown in Fig. 12 as a function of the normalized thickness t/a. It shows that the phase angle increases with an increasing thickness of the septum. If we replace the bifurcated waveguide section by an equivalent empty waveguide of length ℓ short circuited

Table 3. Scattering parameters of semi-infinite septum of finite thickness. Septum thickness t = .254 mm, a = 7.112 mm, f = 30 GHz.

M	$S_{11}(1,1)$	$S_{31}(1,1)$	$S_{13}(1,1)$	$S_{33}(1,1)$
1	(1.000,2.489)	(.6895,1.244)	(1.029,-.326)	(.3836,-1.179)
2	(1.000,2.490)	(.6889,1.245)	(1.027,-.325)	(.3826,-1.179)
3	(1.000,2.490)	(.6888,1.245)	(1.027,-.325)	(.3823,-1.179)
4	(1.000,2.490)	(.6889,1.245)	(1.027,-.325)	(.3822,-1.179)
5	(1.000,2.490)	(.6889,1.245)	(1.026,-.325)	(.3821,-1.179)
6	(1.000,2.490)	(.6889,1.245)	(1.026,-.325)	(.3820,-1.179)

Table 4. Scattering parameters of semi-infinite septum of finite thickness. Septum thickness t = .254 mm, a = 7.112 mm, f = 40 GHz.

M	$S_{11}(1,1)$	$S_{31}(1,1)$	$S_{13}(1,1)$	$S_{33}(1,1)$
1	(1.000,1.839)	(1.340,.290)	(.6982,-.651)	(.5702,-2.179)
2	(1.000,1.841)	(1.340,.921)	(.6977,-.649)	(.5694,-2.179)
3	(1.000,1.841)	(1.340,.921)	(.6976,-.649)	(.5692,-2.179)
4	(1.000,1.841)	(1.340,.921)	(.6975,-.649)	(.5690,-2.179)
5	(1.000,1.841)	(1.340,.921)	(.6974,-.649)	(.5690,-2.179)
6	(1.000,1.841)	(1.340,.921)	(.6974,-.648)	(.5689,-2.179)

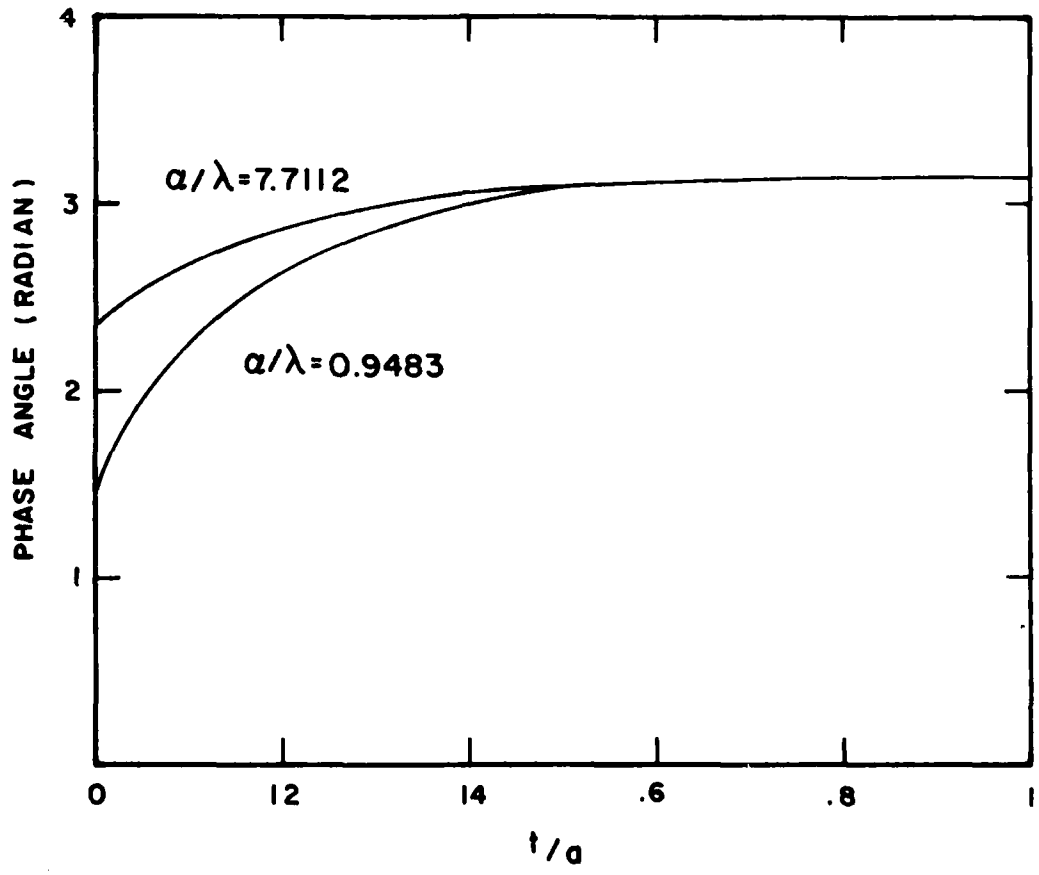

Fig. 12. Thickness effect of semi-infinite septum (phase angle of S_{11} versus normalized thickness t/a).

at the very end, the thickness effect means that ℓ decreases with an increasing t. This is because when t increases, the narrow-waveguide sections become smaller and less energy is stored in them.

The effect of thickness on the scattering characteristics of a finite-length septum is more explicit. It is no longer true in this case that all the electromagnetic energy is reflected; instead, part of the energy is transmitted through the cut-off waveguide by way of evanescent mode coupling. It is obvious that the increase of septum thickness would cause more reflection and less transmission. This phenomenon is well shown by the results summarized in Table 5.

Finally, the thickness effect of the septum on the performance of the filter circuits is demonstrated by a filter designed on a purely metallic sheet. The performance of the bandpass filter is first optimized on a 5-mil thick sheet. Then using the same design parameters, the filter response is calculated for the filter circuits by varying the thickness of the metal sheet. The results are plotted in Fig. 13. The most noticeable effect is that the center frequency shifts upward approximately 1 MHz per 1-mil increase in thickness. This effect is mainly due to the fact that the increase of septum thickness effectively shortens the equivalent length of the resonators formed between two septa, and thus causes the resonant frequency to shift upward. In addition to this effect, there are some other effects. For example, the passband

Table 5. Scattering parameters of finite-length septum of finite thickness. (a = 7.112 mm, d = 0.5 mm)

	f = 30 GHz		f = 40 GHz	
t(mm)	S_{11}	S_{21}	S_{11}	S_{21}
0.0	(.7519,2.221)	(.6574,0.650)	(.5453,1.825)	(.8359,0.256)
0.002	(.7518,2.222)	(.6593,0.651)	(.5446,1.829)	(.8387,0.258)
0.02	(.7663,2.244)	(.6436,0.676)	(.5589,1.846)	(.8295,0.279)
0.127	(.8161,2.335)	(.5793,0.768)	(.6172,1.933)	(.7872,0.367)
0.254	(.8552,2.418)	(.5190,0.849)	(.6712,2.022)	(.7415,0.454)
1.0	(.9603,2.730)	(.2788,1.160)	(.8758,2.430)	(.4823,0.861)
2.0	(.9934,2.951)	(.1120,1.381)	(.9771,2.804)	(.2092,1.234)

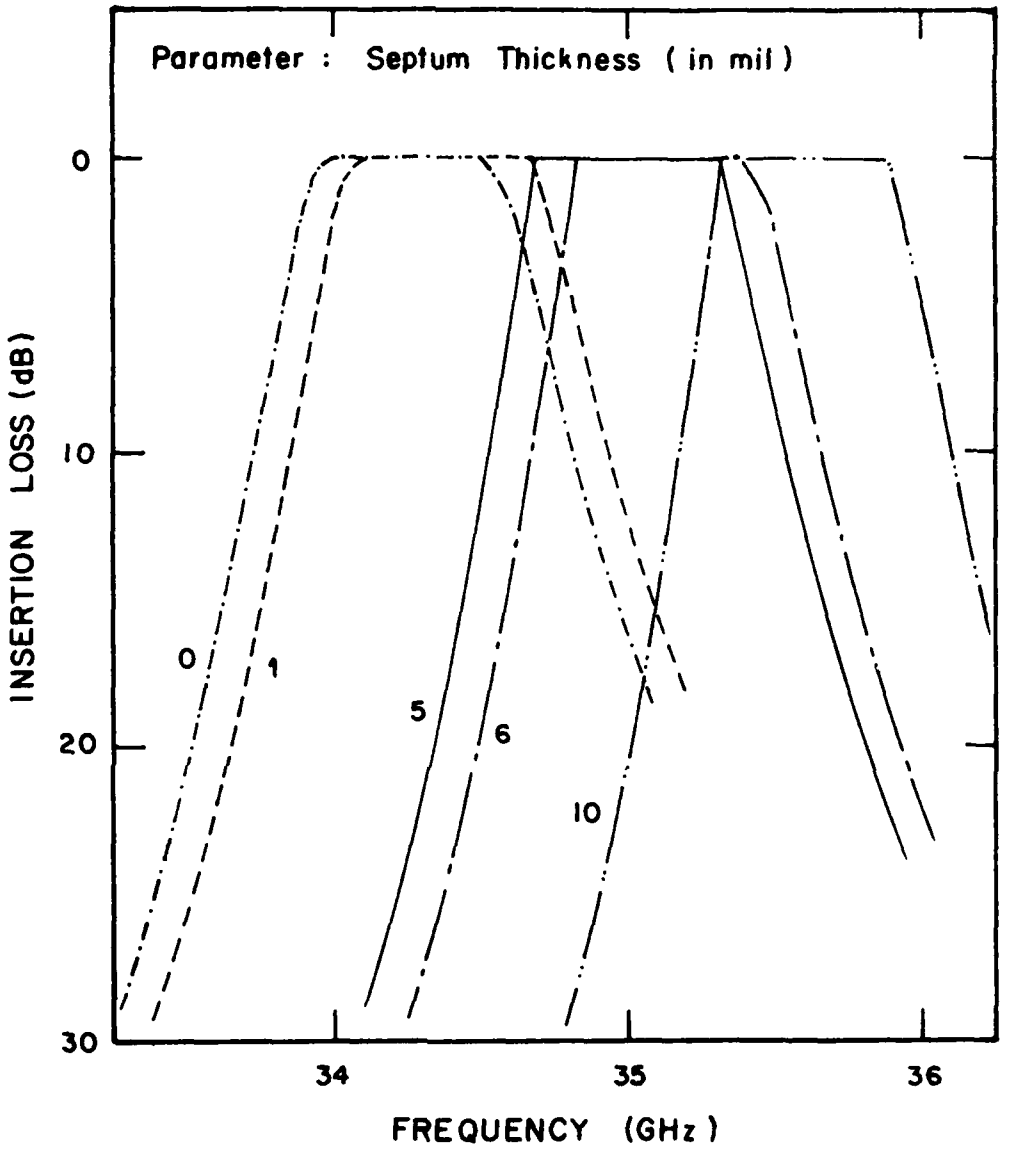

Fig. 13. Thickness effects on filter performance (second filter design in Table 6.)

ripple increases perceptibly and the bandwidth shrinks slightly due to changes in coupling between resonators.

D. Design Examples

Several E-plane filters employing septa with finite thickness have been designed and tested at microwave frequencies by Konishi, et al. [1] and Tajima, et al. [2]. The validity of this analysis is checked by using their design data to calculate the filter responses. The results are shown in Fig. 14 in comparison with their measurements. Good agreement is observed.

Filters for Ka-band and W-band applications are designed with pure metal structures. Typical design parameters are tabulated in Table 6. There are certain advantages inherent to these structures: First, there is no dielectric loss involved. Second, the grooves for supporting the circuits in the waveguide are totally filled with metal; therefore, the error due to the grooves is reduced. It is expected that these filters are superior to those made in unilateral and bilateral finline configurations.

IV. CONCLUSIONS

A class of low-loss waveguide filters can be designed using the unified CAD algorithm developed in this study. The filter structure is composed of a printed circuit inserted in a waveguide parallel to the E-plane. This circuit is designed either on a purely metallic sheet or on various finline structures. It consists

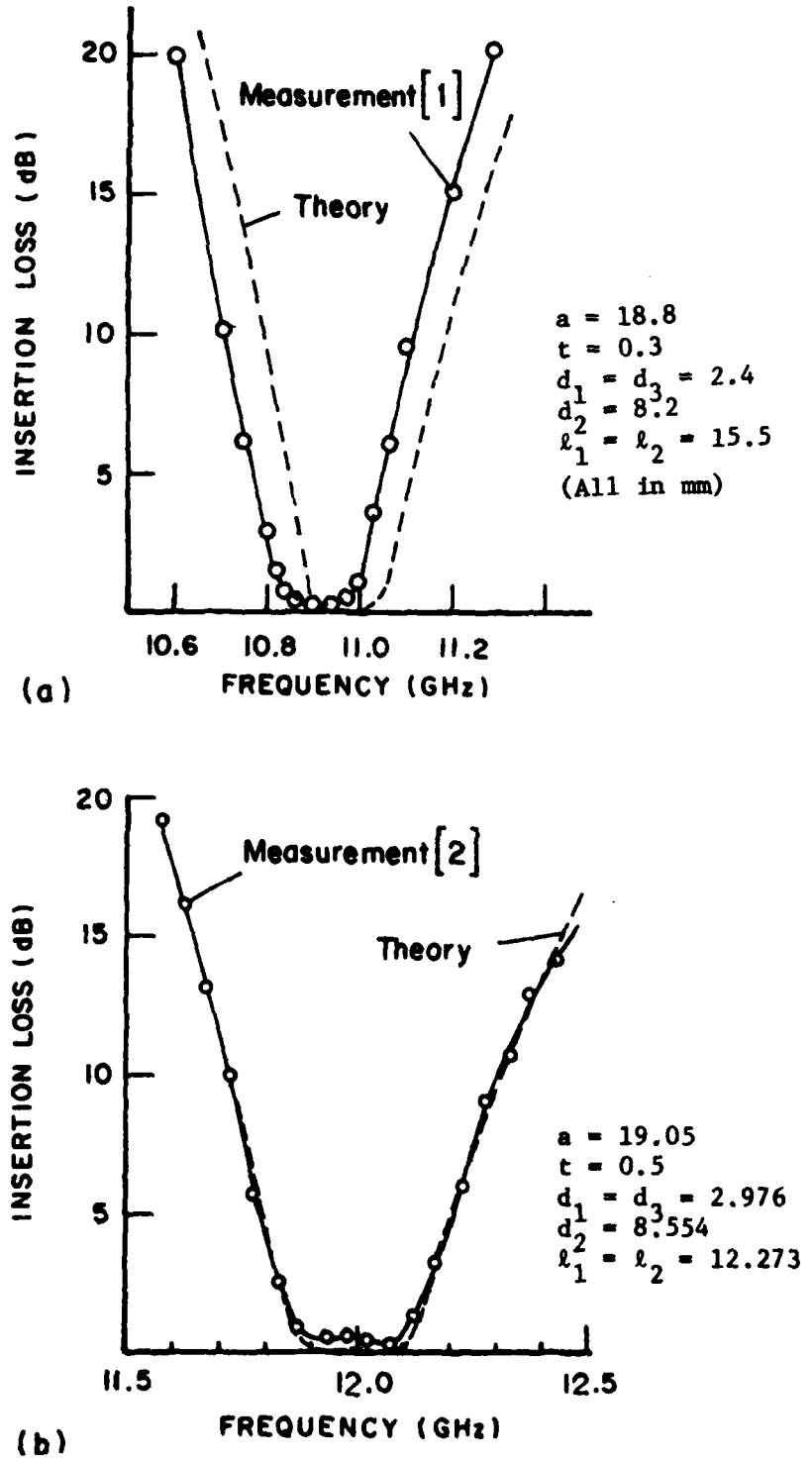

Fig. 14. Frequency response of E-plane filters using metal sheets of finite thickness.

Table 6. Design parameters for filters using finite-thickness septa.

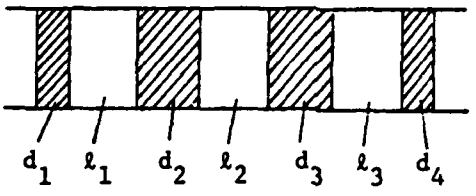

Freq. Band	t	$d_1 = d_4$ (mm)	$d_2 = d_3$ (mm)	$\ell_1 = \ell_3$ (mm)	ℓ_2	Passband* (GHz)
Ka	0.005"	2.1286	6.0126	2.6640	2.6224	38.5-39.2
Ka	0.005"	1.6641	4.8211	3.6178	3.6108	34.75-35.25
W	0.002"	.59354	1.7130	1.2999	1.2977	97.3-98.7
W	0.002"	.74264	2.1114	.96107	.94625	107.8-109.8

* Passband ripple is small than 0.1 dB.

of several resonators separated by inductive strips; such a configuration is highly suitable for low-cost mass production.

The analysis portion of the CAD algorithm is based on the combination of two methods, viz, the residue-calculus technique and the generalized scattering matrix method. The former is first applied to obtain closed-form expressions for the scattering parameters of a junction created by a semi-infinite septum in the waveguide. Based on this information, the latter is then applied to obtain the composite scattering parameters for a filter structure. This analysis is mathematically exact and numerically very efficient because the convergence is guaranteed.

Filters have been designed and tested in Ka band using bilateral and unilateral configurations. Measured characteristics agree well with theoretical data. Extensive experiments show that the bilateral constructure is more promising than the unilateral structure.

The thickness effect of the metal sheet is also discussed. Neglecting this effect in the design causes a shift in the center frequency and degrades the performance of the filter. The analysis taking into account the metal thickness has been incorporated in the design procedure, which is believed to be useful for design of filters above Ka band.

APPENDIX A. EXPRESSIONS FOR EIGENFUNCTIONS

The function ϕ_{in} has to satisfy the second-order ordinary differential equation

$$\frac{\partial^2 \phi_{in}}{\partial x^2} - k_{xn}^2 \phi_{in} = 0 \tag{25}$$

and the boundary conditions at $x = 0$ and $x = a$. The wave number in the x direction, k_{xn}, is related to the propagation constant γ_n via the dispersion relation

$$\gamma_n^2 - k_{xn}^2 = \varepsilon_r k_o^2 \tag{26}$$

where k_o is the free-space wave number. The expressions for ϕ_{in} and γ_{in} of different geometries are given in the following :

Metallic E-Plane Structure

$$\begin{aligned}
\phi_{1n}(x) &= \sqrt{\frac{2}{a}} \sin\frac{n\pi}{a}x \\
\phi_{2n}(x) &= \sqrt{\frac{2}{b}} \sin\frac{n\pi}{b}x \\
\phi_{3n}(x) &= \sqrt{\frac{2}{c}} \sin\frac{n\pi}{c}(a-x) \\
\gamma_{1n} &= \sqrt{k_o^2 - \left(\frac{n\pi}{a}\right)^2} \\
\gamma_{2n} &= \sqrt{k_o^2 - \left(\frac{n\pi}{b}\right)^2} \\
\gamma_{3n} &= \sqrt{k_o^2 - \left(\frac{n\pi}{c}\right)^2}
\end{aligned} \tag{27}$$

Bilateral Finline Structure

$$\phi_{1n}(x) = \begin{cases} B_n \cos\xi_n x & , \ 0 < x < b \\ B_n \dfrac{\cos\xi_n b}{\sinh\eta_n c} \sinh\eta_n (a-x) & , \ b < x < a \end{cases}$$

$$\phi_{2n}(x) = \sqrt{\frac{2}{b}} \sin\frac{n\pi}{b}x$$

$$\phi_{3n}(x) = \sqrt{\frac{2}{c}} \sin\frac{n\pi}{c}(a-x)$$

$$\gamma_{1n} = \sqrt{\varepsilon_r k_o^2 - \xi_n^2} \quad = \sqrt{k_o^2 - \eta_n^2} \tag{28}$$

$$\gamma_{2n} = -\sqrt{\varepsilon_r k_o^2 - \left(\frac{n\pi}{b}\right)^2}$$

$$\gamma_{3n} = -\sqrt{k_o^2 - \left(\frac{n\pi}{c}\right)^2}$$

where

$$B_n = \left[\frac{b}{2} + \frac{c}{2}\left(\frac{\cos\xi_n b}{\sin\eta_n c}\right)^2 + \frac{\sin\xi_n b\cos\xi_n b}{2\xi_n} - \frac{\sin\eta_n c\cos\eta_n c}{\eta_n}\left(\frac{\cos\xi_n b}{\sin\eta_n c}\right)^2\right]^{-\frac{1}{2}}$$

and ξ_n and η_n are obtained from the simultaneous equations:

$$\xi_n^2 - \varepsilon_r k_o^2 = \eta_n^2 - k_o^2 \tag{29a}$$

$$\xi_n \tan\xi_n b = \eta_n \cot\eta_n c \tag{29b}$$

Unilateral Finline Structure

$$\phi_{1n}(x) = \begin{cases} B_n \sin\eta_n x & ,0 < x < e_1 \\ B_n\left[\sin\eta_n e_1 \cos\xi_n(x-e_1) + \frac{\eta_n}{\xi_n}\cos\eta_n e_1 \sin\xi_n(x-e_1)\right] & ,e_1 < x < b \\ B_n C_n \sin\eta_n(a-x) & ,b < x < a \end{cases}$$

$$\phi_{2n}(x) = \begin{cases} B_n' \sin\eta_n' x & ,0 < x < e_1 \\ B_n' \dfrac{\sin\eta_n' e_1}{\sin\xi_n' e_2} \sin\xi_n'(b-x) & ,e_1 < x < b \end{cases}$$

$$\phi_{3n}(x) = \sin\frac{n\pi}{c}(a-x)$$

$$\gamma_{1n} = \sqrt{\varepsilon_r k_o^2 - \xi_n^2} \quad = \sqrt{k_o^2 - \eta_n^2} \tag{30}$$

$$\gamma_{2n} = -\sqrt{\varepsilon_r k_o^2 - \xi_n'^2} \quad = -\sqrt{k_o^2 - \eta_n'^2}$$

$$\gamma_{3n} = -\sqrt{k_o^2 - \left(\frac{n\pi}{c}\right)^2}$$

where

$$B_n = \left[\frac{d}{2} - \frac{\sin\eta_n e_1 \cos\eta_n e_1}{2\eta_n} + \frac{\eta_n^2 e_1}{2}\left(\frac{\sin^2\eta_n e_1}{\eta_n^2} + \frac{\cos^2\eta_n e_1}{\xi_n^2}\right) + \frac{C_n\eta_n^2 \sin\xi_n e_2}{2\xi_n}\left(\frac{\sin\eta_n e_1 \sin\eta_n c}{\eta_n^2} + \frac{\cos\eta_n e_1 \cos\eta_n c}{\xi_n^2}\right) + C_n^2\left(\frac{c}{2} - \frac{\sin\eta_n c \cos\eta_n c}{2\eta_n}\right)\right]^{\frac{-1}{2}}$$

$$C_n = \frac{\eta_n}{\sin\eta_n c}\left(\frac{\sin\eta_n e_1 \cos\xi_n e_2}{\eta_n} + \frac{\sin\xi_n e_2 \cos\eta_n e_1}{\xi_n}\right)$$

$$B_n' = \left[\frac{e_1}{2} - \frac{\sin\eta_n' e_1 \cos\eta_n' e_1}{2\eta_n'} + \left(\frac{e_2}{2} - \frac{\sin\xi_n' e_2 \cos\xi_n' e_2}{2\xi_n'}\right)\left(\frac{\sin\eta_n' e_1}{\sin\xi_n' e_2}\right)^2\right]^{\frac{-1}{2}}$$

and ξ_n, η_n, ξ_n', and η_n' are obtained by solving the following simultaneous equations:

$$\xi_n^2 - \varepsilon_r k_o^2 = \eta_n^2 - k_o^2 \tag{31a}$$

$$\frac{\xi_n \tan\eta_n e_1 + \eta_n \tan\xi_n e_2}{\xi_n \tan\eta_n e_1 \tan\xi_n e_2 - \eta_n} = \frac{\tan\eta_n c}{\eta_n} \tag{31b}$$

$$\xi_n'^2 - \varepsilon_r k_o^2 = \eta_n'^2 - k_o^2 \tag{31c}$$

$$\xi_n' \tan\eta_n' e_1 + \eta_n' \tan\xi_n' e_2 = 0 \tag{31d}$$

APPENDIX B. EXPRESSIONS FOR H_n, F_n, AND G_n

The coefficients H_n, F_n, and G_n are related to the structure geometry and the field distribution in regions I, II, and III respectively. They are derived from the overlapping integrals

$$\int_0^b \phi_{1m}(x)\ \phi_{2n}(x)\ dx = \frac{H_m F_n}{\gamma_{2n}^2 - \gamma_{1m}^2} \tag{32a}$$

$$\int_b^a \phi_{1m}(x)\ \phi_{3n}(x)\ dx = \frac{H_m G_n}{\gamma_{3n}^2 - \gamma_{1m}^2} \tag{32b}$$

where $\phi_{1n}(x)$, $\phi_{2n}(x)$, and $\phi_{3n}(x)$ are the n-th order orthonormal eigenfunctions for the E_y fields in regions I, II, and III, respectively (refer to Fig. 3). The expressions for H_n, F_n, and G_n of different geometries are given in the following.

Metallic E-Plane Structure

$$\begin{aligned} H_n &= \sqrt{\frac{2}{a}} \sin\frac{n\pi b}{a} \\ F_n &= (-1)^n \sqrt{\frac{2}{b}} \frac{n\pi}{b} \\ G_n &= (-1)^n \sqrt{\frac{2}{c}} \frac{n\pi}{c} \end{aligned} \tag{33}$$

Bilateral Finline Structure

$$\begin{aligned} H_n &= B_n \cos\xi_n b \\ F_n &= (-1)^n \sqrt{\frac{2}{b}}\ \frac{(n - 1/2)\pi}{b} \\ G_n &= (-1)^n \sqrt{\frac{2}{c}}\ \frac{n\pi}{c} \end{aligned} \tag{34}$$

where B_n and ξ_n are defined in equations (28-29)

Unilateral Finline Structure

$$H_n = B_n C_n \sin\eta_n c$$

$$F_n = -B_n' \xi_n' \frac{\sin\eta_n' e_1}{\sin\xi_n' e_2} \qquad (35)$$

$$G_n = (-1)^n \sqrt{\frac{2}{c}} \frac{n\pi}{c}$$

where B_n, C_n, η_n, B_n', ξ_n', and η_n' are defined in equations (30-31).

APPENDIX C. ALTERNATIVE SET OF SCATTERING PARAMETERS

$$S_{11}(m,p) = \frac{-\gamma_{1p}H_m}{\gamma_{1m}H_p} e^{L(\gamma_{1m}+\gamma_{1p})} \frac{(\gamma_{1p}-\gamma_{1p})}{(\gamma_{1p}+\gamma_{1m})} g(\gamma_{1m}, \gamma_{1p}) \quad (36a)$$

$$S_{21}(m,p) = \frac{2\gamma_{1p}}{H_p F_m} e^{L(\gamma_{2m}+\gamma_{1p})} \frac{(\gamma_{1p}-\gamma_{1p})(\gamma_{2m}-\gamma_{2m})}{(\gamma_{1p}+\gamma_{2m})} g(\gamma_{2m},\gamma_{1p}) \quad (36b)$$

$$S_{31}(m,p) = \frac{2\gamma_{1p}}{H_p G_m} e^{L(\gamma_{3m}+\gamma_{1p})} \frac{(\gamma_{1p}-\gamma_{1p})(\gamma_{3m}-\gamma_{3m})}{(\gamma_{1p}+\gamma_{3m})} g(\gamma_{3m},\gamma_{1p}) \quad (36c)$$

$$S_{12}(m,p) = \frac{-H_m F_p}{2\gamma_{1m}} e^{L(\gamma_{2p}+\gamma_{1m})} \frac{1}{(\gamma_{2p}+\gamma_{1m})} g(\gamma_{1m},\gamma_{2p}) \quad (36d)$$

$$S_{22}(m,p) = \frac{-F_p}{F_m} e^{L(\gamma_{2m}+\gamma_{2p})} \frac{(\gamma_{2m}-\gamma_{2m})}{(\gamma_{2m}+\gamma_{2p})} g(\gamma_{2m},\gamma_{2p}) \quad (36e)$$

$$S_{32}(m,p) = \frac{-F_p}{G_m} e^{L(\gamma_{3m}+\gamma_{2p})} \frac{(\gamma_{3m}-\gamma_{3m})}{(\gamma_{3m}+\gamma_{2p})} g(\gamma_{3m},\gamma_{2p}) \quad (36f)$$

$$S_{13}(m,p) = \frac{-H_m G_p}{2\gamma_{1m}} e^{L(\gamma_{3p}+\gamma_{1m})} \frac{1}{(\gamma_{3p}+\gamma_{1m})} g(\gamma_{1m},\gamma_{3p}) \quad (36g)$$

$$S_{23}(m,p) = \frac{-G_p}{F_m} e^{L(\gamma_{2m}+\gamma_{3p})} \frac{(\gamma_{2m}-\gamma_{2m})}{(\gamma_{2m}+\gamma_{3p})} g(\gamma_{2m},\gamma_{3p}) \quad (36h)$$

$$S_{33}(m,p) = \frac{-G_p}{G_m} e^{L(\gamma_{3m}+\gamma_{3p})} \frac{(\gamma_{3m}-\gamma_{3m})}{(\gamma_{3m}+\gamma_{3p})} g(\gamma_{3m},\gamma_{3p}) \quad (36i)$$

$$g(\alpha,\beta) = \prod_{n=1}^{\infty} \frac{(\gamma_{1n}+\alpha)(\gamma_{2n}+\beta)(\gamma_{3n}+\beta)}{(\gamma_{1n}-\beta)(\gamma_{2n}-\alpha)(\gamma_{3n}-\alpha)}$$

APPENDIX D. EQUIVALENT CIRCUIT OF A SEPTUM

The equivalent T-network for a finite-length septum is shown in Fig. 15 . The values of the normalized reactances x_s and x_p are to be calculated from the scattering parameters of a septum of length, say, D. Let the scattering matrix of the fundamental mode be

$$S = \begin{bmatrix} S_{11} & S_{12} \\ S_{21} & S_{22} \end{bmatrix} \tag{37}$$

For this reciprocal lossless two-port device, the following relations hold:

$$\begin{aligned} S_{12} &= S_{21} \\ S_{11} &= S_{22} \\ |S_{11}|^2 + |S_{12}|^2 &= 1 \end{aligned} \tag{38}$$

These relations provide useful error-checking criteria for the numerical calculations.

If we convert the scattering matrix into impedance matrix and equate it to the impedance matrix of the equivalent T network, we have

$$[\bar{Z}] = [I + S]\,[I - S]^{-1} = \begin{bmatrix} (jx_s + jx_p) & jx_p \\ jx_p & (jx_s + jx_p) \end{bmatrix} \tag{39}$$

where I is the identity matrix. By equating the elements in the matrix on both sides, we obtain x_s and x_p as:

$$jx_s = \frac{1 - S_{12} + S_{11}}{1 - S_{11} + S_{12}} \tag{40a}$$

$$jx_p = \frac{2S_{12}}{(1 - S_{11})^2 - S_{12}^2} \tag{40b}$$

The curves in Fig 15 are calculated values for x_s and x_p as a function of septum length D with frequency as parameters.

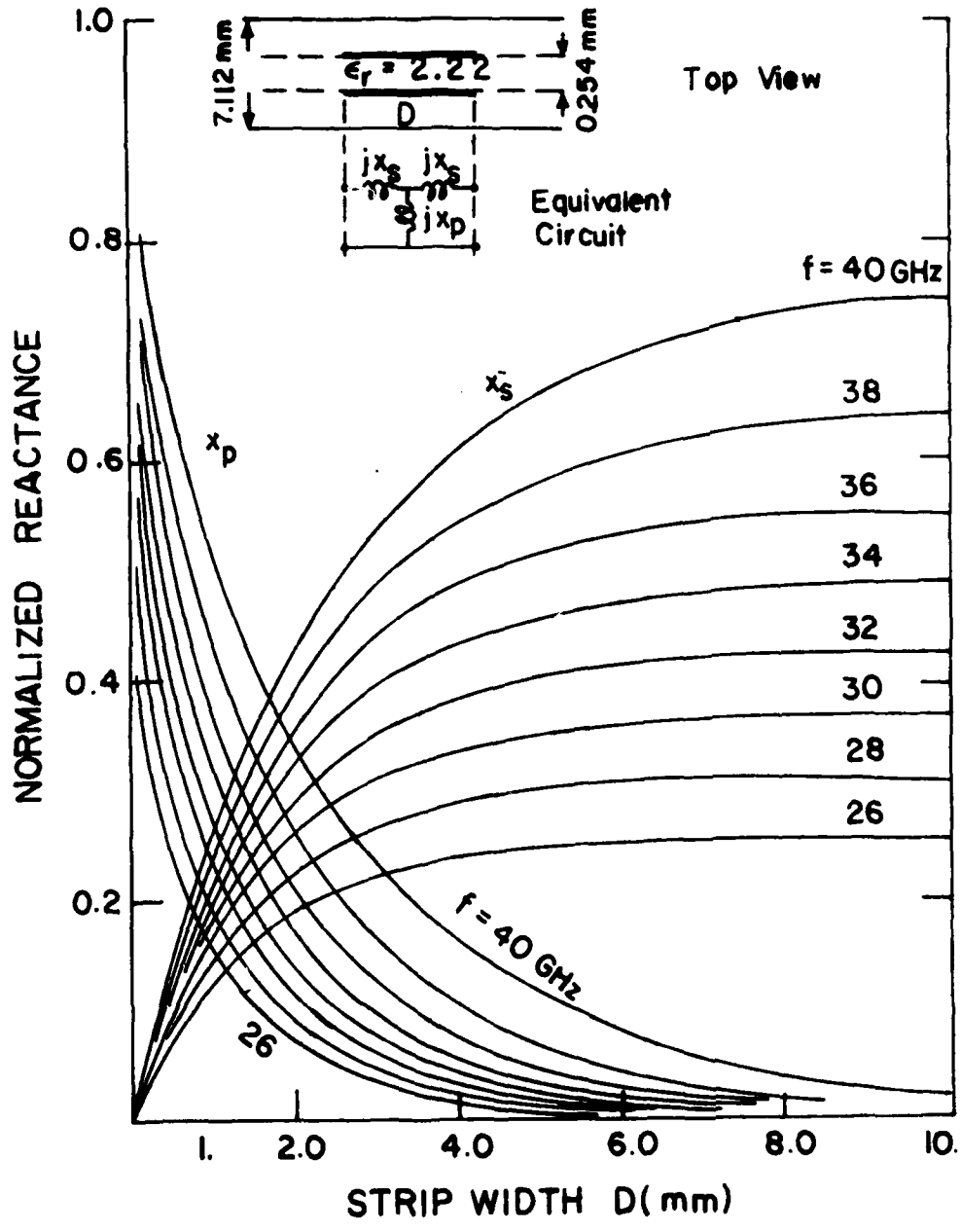

Fig. 15. Equivalent T network and parameters for finete-length septa.

BIBLIOGRAPHY

1. Y. Konishi and K. Uenakada, "The design of a bandpass filter with inductive strip-planar circuit mounted in waveguide," IEEE Trans. Microwave Theory Tech., Vol. MTT-22, pp. 869-873, Oct. 1974.

2. Y. Tajima and Y. Sawayama, "Design and analysis of a waveguide-sandwich microwave filter," IEEE Trans. Microwave Theory Tech., Vol. MTT-22, pp. 839-841, Sept. 1974.

3. P. J. Meier, "Integrated fin-line millimeter components," IEEE Trans. Microwave Theory Tech., Vol. MTT-22, pp. 1209-1216, Dec. 1974.

4. A. M. K. Saad and K. Schunemann, "Design and performance of fin-line bandpass filters," 9th European Microwave Conference, Brighton, England, Sept. 17-20, 1979.

5. F. Arndt, et al., "Low-insertion-loss fin-line filters for millimeter-wave applications," 11th European Microwave Conference, Amsterdam, The Netherlands, Sept. 7-10, 1981, pp. 309-314.

6. R. Mittra, T. Itoh and T. Li, "Analytical and numerical studies of the relative convergence phenomenon arising in the solution of an integral equation by the moment method," IEEE Trans. Microwave Theory Tech., Vol. MTT-20, pp. 96-104, 1972.

7. Y. C. Shih, T. Itoh and L. Bui, "Computer-aided design of millimeter-wave E-plane filters," Accepted for publication, IEEE Trans. Microwave Theory Tech.

8. R. Mittra and S. W. Lee, Analytical Techniques in the Theory of Guided Waves (New York: Macmillan, 1971), pp. 45-54.

9. Ibid, pp. 207-217.

10. C. F. Vanblaricum, Jr. and R. Mittra, "A modified residue-calculus technique for solving a class of boundary value problems - part II: Waveguide phased arrays, modulated surfaces, and diffraction gratings," IEEE Trans. Microwave Tech., Vol. MTT-17, pp. 310-319, June 1969.

11. R. Mittra and S. W. Lee, Analytical Techniques in the Theory of Guided Waves (New York: Macmillan, 1971), pp. 4-11.

12. T. E. Rozzi and W. F. G. Mecklenbrauker, "Wide-band network modeling of interacting inductive irises and steps," IEEE Trans. Microwave Theory Tech., Vol. MTT-23, pp. 235-244, 1975.

13. Routin ZXMIN, IMSL Library 3 (for CDC Cyber 70/6000/7000 series). See IMSL Library Manual.

14. J. W. Bandler, "Optimization method for computer-aided design," IEEE Trans. Microwave Theory Tech., Vol. MTT-17, pp. 533-562, August 1969.

15. P. J. Meier, "Equivalent relative permittivity and unloaded Q factor of integrated fin-line," Electronics Letters, Vol. 9, No. 7, pp. 162-163, April 1973.

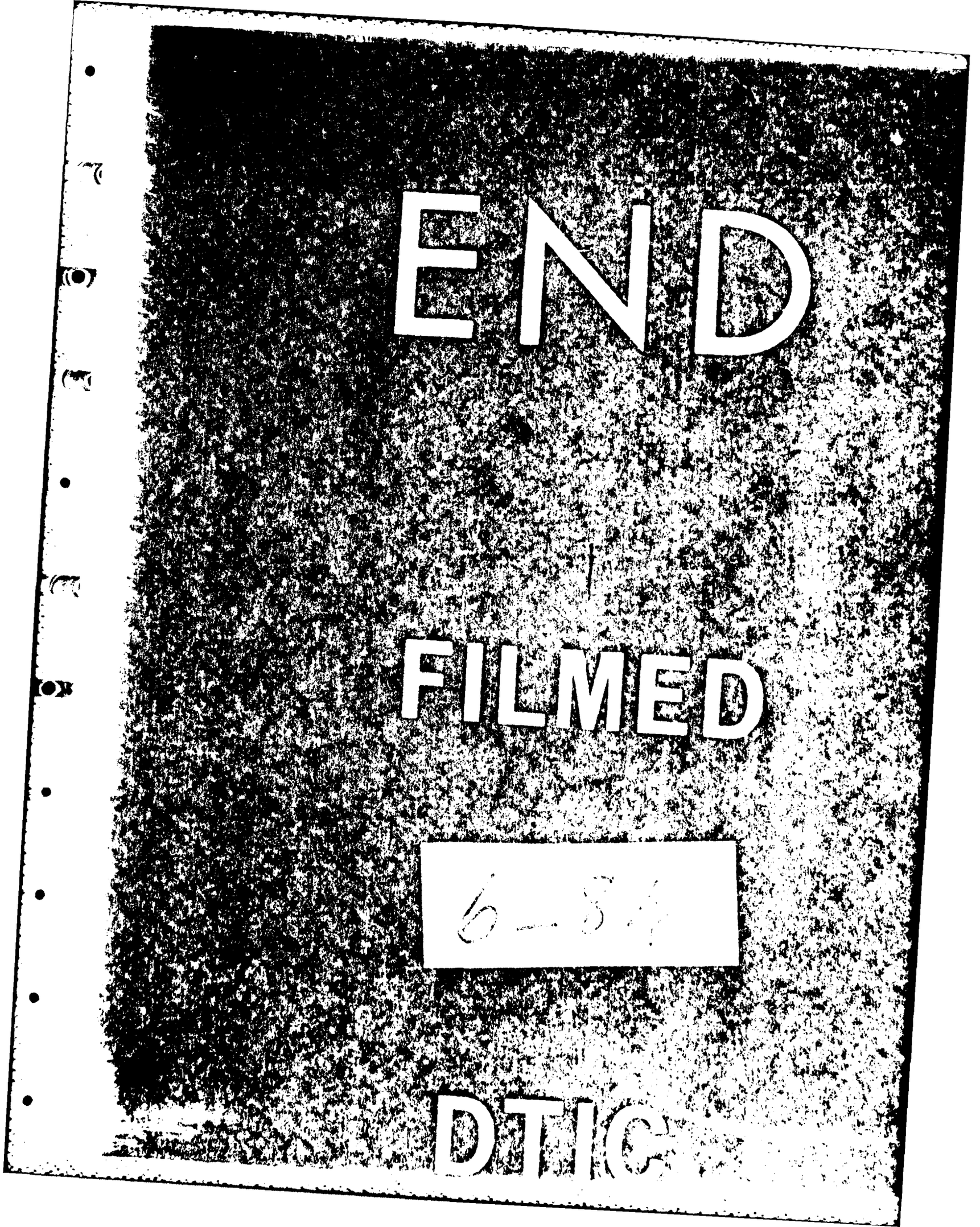
END
FILMED
6-84
DTIC